# MODELING OF NONLINEAR DYNAMICAL SYSTEMS USING KOOPMAN OPERATOR THEORY

A THESIS SUBMITTED TO THE GRADUATE DIVISION OF THE UNIVERSITY OF HAWAIʻI AT MĀNOA IN PARTIAL FULFILLMENT OF THE REQUIREMENTS FOR THE DEGREE OF

MASTER OF SCIENCE

IN

MECHANICAL ENGINEERING

DECEMBER 2021

By

Gregory A Snyder

Thesis Committee:

Zhuoyuan Song, Chairperson
Dilmurat Azimov
Monique Chyba

Keywords: Dynamical System, Koopman Operator, Dynamic Mode Decomposition, Control System Theory

# ACKNOWLEDGMENTS

First and foremost, I would like to thank my advisor, Dr. Zhuoyuan Song, who welcomed me to the RAN lab and supported my research. I would also like to thank all of my colleagues in the RAN lab and fellow students in the Mechanical engineering department who helped motivate me throughout the pandemic to continue working and learning. I also owe a huge thank you to Dr. Philip von Doetinchem for the invaluable experience I gained as a physics lab teaching assistant. I would also like to thank my colleagues at the CANS lab at Kirkland AFB with the AFRL, for encouragement and the valuable research experiences they gave me. Last but not least, I would like to thank my MS thesis committee: Dr. Dilmurat Azimov and Dr. Monique Chyba for their help and insight.

# ABSTRACT

The dynamics of most mechanical systems tends to incorporate nonlinear functions and behaviors to model complex systems. Due to the complexity of some of these systems, only analytical solutions can be found to model, optimize and control them however the costs of doing so are not always feasible. To solve these nonlinear systems we usually need to take approximations through linearization which can lead to a loss of fidelity in modeling systems to accommodate the computing power needed to solve them.

This work is the culmination of research and study involving the use of a data-driven spectral method to generate a linear approximation of nonlinear systems using Koopman operator theory. The Koopman operator is an infinite dimensional operator that 'lifts' the nonlinear behavior of a system to a higher dimensional state. In this lifted state, the evolution of these nonlinear dynamics progresses linearily. This work investigates the use of data driven methods such as dynamic mode decomposition (DMD), and one of its variants, to find the Koopman operator of some nonlinear dynamical systems.

In this work we initially go through decomposing the linear dynamics of the above systems using DMD on two sample systems to verify the efficacy of this method of finding the Koopman operator before lifting the dynamics. Using a variant of DMD, extended dynamic mode decomposition, we decompose the lifted non-linear dynamics of a pendulum and cart-pendulum system to find the leading Koopman eigenfunctions to approximate a lower, finite-dimensional representation of the discovered dynamics. We used these methods of reconstruction on controlled and uncontrolled data of the sample systems to compare the observed dynamics to evaluate the reconstruction on a wider breadth of behaviors a system can produce. Using these reconstructed states analyze the limitations and discuss possible improvements to these methods of finding the Koopman operator.

# TABLE OF CONTENTS

# LIST OF FIGURES

# CHAPTER 1
# INTRODUCTION

Advancements in data-driven systems and in computing have given rise to Koopman operator theory, an alternate view of how to describe dynamical systems. Using the Koopman operator, we can identity intrinsic states and alternative coordinate systems where non-linear dynamical systems can appear linear. Obtaining new linear representations of nonlinear systems can potentially make far reaching changes in how we can model, predict and control like systems. This chapter provides a brief overview of dynamical systems a brief overview of the Koopman operator and a literature review of recent works and applications of the Koopman operator in modeling dynamical systems.

## 1.1 History of the Koopman Operator

The Koopman operatory originated with the early work by Koopman [1] on the introduction of an operator that produces a unitary transformation in Hamiltonian dynamical systems. This lead to further work with spectral theory with John von Neumann in 1932 [2] which further described a spectrum associated with the operator Koopman discovered the year prior in [1]. This work was then relatively untouched for 70 years as there was no immediate application of this analytical method of modeling dynamical systems as it would be too difficult to continue calculations without assistance. In the early 2000's the Koopman operator saw a reemergence in the work done by Igor Mezic in [3,4] where he showed how we can can reduce and reconstruct high dimensional state-spaces from data and use significant eigenvalues of the Koopman operator to detect and determine trends in the dynamics of data that can appear chaotic which can be referred to as Koopman modes.

Later, Rowley et al. [5] used the Koopman operator and applied it to complex fluid flow and showed how capturing relevant structures discretely in a Koopman mode decomposition (KMD) which showed a data-driven method of showing a connection between measurements taken of a system and its associated dynamics in the state-space. This work showed that KMD can be found through dimensional reduction algorithms developed by Schmid et al. [6]. In [6], Schmid et al. developed a data-driven method of determining the dynamic information from a flow field past a cylinder to determine the dominant modes to find describe the dynamics in a process called dynamic mode decomposition. Together, the work by Schmid [6] and Rowley [5] have developed a close relationship between KMD and DMD and the two decomposition techniques have become popular in investigating nonlinear flows in particular

[7–10] as well as other fields which will be further described in section 1.3.

## 1.2 Background on Dynamical Systems

This work pertains to the implementation of Koopman operator theory on dynamical systems to propagate non-linear dynamical equations with a data-driven approximation method. Conventionally, a non-linear dynamical system consists of a set of states and a function or rule that governs how the states propagate either forward in time or with respect to each other [9, 11]. This can be described in a continuous and a discrete method.

For a generic continuous system

$$\frac{d}{dt}\mathbf{x}(t) = F(\mathbf{x}(t), t; \mu), \tag{1.1}$$

$\mathbf{x}(t) \in \mathbb{R}^n$ is the vector holding the states of the dynamical system at time $t$, $n$ is the number of states that define the system, $\mu$ is a set of parameters for the system dynamics, and $F(\cdot)$ is the rule describing the evolution of the state in a continuous sense. These continuous-time dynamics can also be modeled in a respective discrete-time representation where the system can be evaluated at every finite time interval, $\Delta t$, which can otherwise be viewed as $\mathbf{x}_k = \mathbf{x}(k\Delta t)$ with the subscript $k$.

The evolution of a dynamic system in a discrete-time flow map can be formally portrayed as:

$$\mathbf{x}_{k+1} = f(\mathbf{x}_k), \tag{1.2}$$

by collecting the states at time $t_k$, $k = 1, 2, ..., m$, for $m$ time steps, where $x_k$ is a $n$-dimensional column vector of system states and $\mathbf{x}_{k+1}$ is the states of the system in the time step following $\mathbf{x}_k$ [12–14].

These rules governing how the states of the system advance tend to be nonlinear equations to best simulate most of the systems in practice. An unfortunate quality of nonlinear systems is that their dynamics are difficult to solve analytically. As a result, modern control practices tend to turn to approximations in order to produce a high-fidelity controller for the system. However, if a dynamical system can be expressed with by a linear rule, we can then achieve more accurate predictions of how a system advances in time. We intend to show this using the Koopman operator theory.

## 1.3 Literature review of the Koopman Operator

In this work we explore the application of the Koopman operator to find finite-dimensional linear representation of nonlinear dynamical systems. As aforementioned, the Koopman operator originated with the early work of Koopman with von Neumann in 1932 on the spectrum's that the Koopman operator resides in [2].

Brunton et al. explored the relationship between the Koopman operator and explored multiple observable functions to form a Koopman subspace to develop a Koopman operator [15]. In their work, they showed that the state matrix found by approximating the Koopman operator for specific systems can be used to generate control laws with linear quadratic regression (LQR). Further more, Proctor et al. [14] expanded on their previous work on DMD to create a DMD method with control to extract low-order control models from higher-dimensional systems building the base DMD algorithm. This DMD variant with control(DMDc), is demonstrated to show positive results in the analysis of infections disease data. Proctor et al. [13] introduced a method of finding the Koopman operator of a system that takes into account system's inputs and control (KIC) based on prior work on DMDc. Work has also been done to improve the accuracy of the Koopman operator by 'lifting' the states of the system to a set of observables such that a solution can be found where the data required from DMD is limited, extending the DMD algorithm (EDMD) [16]. Korda et al. [17] presented the use of lifting nonlinear dynamics on augmented states with EDMD and explored finding control laws for systems using model predictive control (MPC). There have also been work done to optimize the methods in which the lifting of dynamics is done through the optimization of the dictionary of functions used to lift the state variables through EDMD with dictionary learning [18].

Applications of the Koopman operator have been explored in the field of robotics, where the operator is used to develop closed-loop controllers for pendulum systems [19]. Kaiser et al. [10] explores the application of the Koopman operator theory in generating energy-based control using a DMD variant with control, extended dynamic mode decomposition with control, and compared it against another method of finding the Koopman operator called the Koopman reduced order nonlinear identification and control (KRONIC). Conversely, the Koopman operator is not a panacea to solving dynamical systems; a recent work by Gonzalez et al. [20] aimed at demonstrating some of the weakness of the Koopman operator and the DMD algorithms and provides alternate approaches to reconstruction.

With the rise in popularity of the Koopman operator there has been many works showing

its viability in approximating nonlinear dynamical systems with this linear operator since works by Mezic [3] and Mezic et al. [17]. More recently, Surana [21] and Surana and Banazuk [22] have explored the use of a Koopman operator and Kalman filter system. As aforementioned, the properties of the Koopman operator is very attractive when exploring the usage of Kalman filter; the data-driven aspects of modeling nonlinear dynamics as linear work in tandem with the restrictions of a conventional Kalman filter. In this work they explore the lifting of the system dynamics and the observation matrices from data of a given system. In [22], Surana and Banazuk demonstrate the usage of a Koopman Kalman filter in a canonical nonlinear dynamical system which instead possess a finite-dimensional Koopman subspace using conventional methods of approximating the operator with its eigenvalues and eigenvectors. In [23], Netto and Mili explore the usage of robust generalized maximum likelihood Koopman operator-based Kalman filter to estimate the states of a power generator and compare their filter against the work of Surana and Banazuk.

In [24] Yeung et al. use deep learning to learn the Koopman operator of nonlinear systems by optimising how the dictionaries used for EDMD are found and used over the specific domains. Using these dictionaries the work analyzes and predicts the dynamics of a glycolytic oscillator several hundred time steps into the future. Other methods of incorporating In [25], Fonzi et al. developed another variant of DMDc for aeroelastic models for morphing wings called algebraic dynamic mode decomposition with control (aDMDc). This variation of DMD takes into account the changing aerostructural dynamics over the body of the airfoils that are being modeled in the work.

## 1.4 Koopman Operator on Dynamical Systems

This work is a detailed summary of an exploration on using the Koopman operator to model a pendulum and cart-pole nonlinear system. In this study we used DMD and EDMD to find the Koopman eigenvecgtors and eigen modes to reconstruct the original state data and took these processes The remainder of this work will be presented in three chapters. The first chapter is a brief background and literature review on dynamical systems and the Koopman operator. The next chapter, 'Koopman Operator for Modeling and Control,' we discuss the mathematics behind the Koopman operator, the DMD algorithm and EDMD algorithms. Following Ch 2, we discuss the experimental setup and the results from the system reconstructions using DMD and EDMD along with the effects of variances on the reference data on the reconstruction

process in 'Implementation of Koopman Operator on Sample Systems'. Lastly we conclude with a brief discussion of our results and a set a direction for future work resulting from this work and the Koopman operator.

# CHAPTER 2
# KOOPMAN OPERATOR FOR MODELING DYNAMICAL SYSTEMS

In this chapter we will discuss the concept and mathematics behind the Koopman operator and the DMD algorithm. Additionally we will discuss the DMD variant, EDMD, and how it relates to discovering the Koopman operator from state-space data.

The Koopman operator is an infinite-dimensional operator that evolves the functions that evolve the state of a dynamical system linearly. In this work, the Koopman operator is computed using data-driven methods such as the dynamic mode decomposition (DMD) algorithm. DMD uses linear measurements of the states of a dynamical system to find the dominant modes of the underlying system from data to reconstruct a linear representation of the evolution of the system.

## 2.1 Introduction to Koopman Operator

The Koopman operator is a linear but infinite dimensional operator that can be defined for an autonomous, discrete time, dynamical system. Unlike the function $f$ shown earlier in (1.2), the Koopman operator advances the measurements of the changes in dynamics over time [11, 13, 17].

## 2.2 Mathematics behind the Koopman Operator

Consider the evolution of a dynamical system $\mathbf{x}_{k+1} = f(\mathbf{x}_k)$ where the rule $f$ maps the state space onto itself, i.e., $f : \mathbb{R}^n \to \mathbb{R}^n$; using Koopman operator theory we define a different rule, $g : \mathbb{R}^n \to \mathbb{M}^{n_y}$, where $n_y$ is the dimension of a nearly infinite column vector defining the dimension of the observable of $\mathbf{x}$ at a given time step. This implies that the Koopman operator is defined for all observables, meaning that the Koopman operator $\mathcal{K}$ is also infinite-dimensional. We will discuss how we can make this a more reasonable attribute later on in this discussion. Here, $g$ is a real-valued, scalar, measurement function which is an element of an infinite-dimensional Hilbert space called an observable. The Koopman operator acts on this observable such that

$$\mathcal{K}_t g = g \circ F(\mathbf{x}(t)), \tag{2.1}$$

$$\mathcal{K}_{\Delta t} g(\mathbf{x}_k) = g(f(\mathbf{x}_k)), \tag{2.2}$$

in a continuous and discreet represention, respectively. In (2.1), the Koopman operator evolves the observable with respect to time in the continuous fashion while in (2.2) the Koopman operator evolves the discrete-time dynamics with respect to $\Delta t$ which is the interval between $k$ and $k+1$ in time series $m$. More details on the connections between these two representations can be found in [10,11,13,17,26]. Equations (2.1) and (2.2) allow us to define an analogue for continuous and discrete-time dynamical systems respectively as the following in a continuously and discreetly as:

$$\frac{d}{dt}g = \mathcal{K}g, \tag{2.3}$$

$$g(\mathbf{x}_{k+1}) = \mathcal{K}_{\Delta t} g(\mathbf{x}_k). \tag{2.4}$$

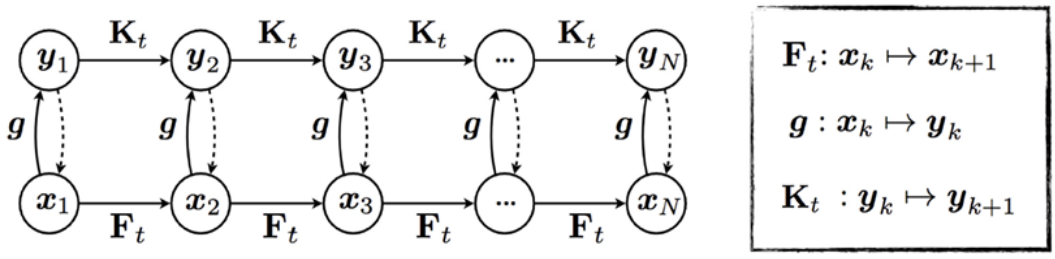


Figure 2.1: Schematic for illustrating the advancement of a dynamical system as defined by the Koopman operator on nonlinear dynamical systems from [27]

However as shown in Fig. 2.1, this operator advances the measurement of the change in dynamics over time [11,13,17]. Reconsidering (1.2) where the rule $F$ maps $x_k$ from $F : \mathbb{R}^n \to \mathbb{R}^n$, using Koopman operator theory we define a different rule, $g$ where $g(\mathbf{x}_k)$ maps $g : \mathbb{R}^n \to \mathbb{M}^{n_y}$ where $n_y$ is the dimension of the near infinite column vector defining the dimension of the observable of that time step of $\mathbf{x}$. This implies that the Koopman operator is defined for all observables meaning that the Koopman Operator $\mathcal{K}$ is also infinite-dimensional. We will discuss how we can make this a more reasonable attribute later on in this discussion. Here $g$ is a real-valued, scalar, measurement function which is an element of an infinite-dimensional Hilbert space called an observable. The Koopman operator acts on this observable, $g$ as:

This work explores the application of the Koopman operator on discreet-time dynamical systems. Due to the linear nature of the Koopman operator, we can perform an eigen

decomposition of $\mathcal{K}$ such that

$$\mathcal{K}\varphi_j(\mathbf{x}_k) = \lambda_j \varphi_j(\mathbf{x}_k), \tag{2.5}$$

where $\lambda$ and $\varphi$ are the Koopman eigenvalue and eigenvector describing the evolution of the Koopman operator. Considering this, the observable, $g(x)$, can be expanded as

$$g(\mathbf{x}) = \begin{bmatrix} g_1(\mathbf{x}) \\ g_2(\mathbf{x}) \\ \vdots \\ g_i(\mathbf{x}) \end{bmatrix} = \sum_{j=1}^{\infty} \varphi_j(\mathbf{x}) \mathbf{v_j}, \tag{2.6}$$

where $\mathbf{v}$ is a coefficient called the Koopman mode associated with its corresponding Koopman eigenvector. This allows us to consider Koopman modes as a projection of the observable:

$$\mathbf{v_j} = \begin{bmatrix} \langle \varphi_j, g_1 \rangle \\ \langle \varphi_j, g_2 \rangle \\ \vdots \\ \langle \varphi_j, g_i \rangle \end{bmatrix}. \tag{2.7}$$

By combining (2.5) and (2.6), one can show the relationship between the observable, $g$, and the Koopman operator, $\mathcal{K}$. However, for all practical proposes, using an infinite-dimensional vector and operator is not always feasible so an approximation of the Koopman operator, $\mathcal{K}$, will be typically used and found from collected data on the system. This approximation allows us to combine the terms in (2.5) and (2.6) to show the relationship between the Koopman modes in $g$ and the Koopman eigenvalues in $\mathcal{K}$

$$\mathcal{K}g(\mathbf{x}_k) = g(f(\mathbf{x}_k)) = \sum_{j=1}^{\infty} \lambda_j \varphi_j(\mathbf{x}) \mathbf{v_j}. \tag{2.8}$$

This shows that the Koopman operator is an iterative set of triples, $\lambda_j, \varphi_j$ and $\mathbf{v_j}$, all of which make up the Koopman mode decomposition when we truncate $\mathcal{K}$ to some $n$ number of finite states we will use for an approximated Koopman operator made up of the most dominant modes in $\mathbf{v}$ [10, 11, 13, 17, 28, 29],

$$\mathcal{K}g(\mathbf{x}_k) \approx \mathcal{K}g(\mathbf{x}_k) = g(f(\mathbf{x}_k)) = \sum_{j=1}^{n} \lambda_j \varphi_j(\mathbf{x}) \mathbf{v_j}. \tag{2.9}$$

This changes how the original dynamical system represented by (x, k, $f$) is transformed into a new dynamical system defined by ($F$, k, $K$). In a graphical sense instead of mapping a system's state from $\mathbf{x}$ to $f(\mathbf{x})$ in the same plane as if this were a simple linear transformation, the Koopman operator updates the observables of the original dynamical system which would take the plane that the original state resides, move it to the new observable plane which transforms the the observable to a new value and then brings that value to a corresponding location on the original state plane. The evolution between these observables is the Koopman operator.

To perform the Koopman analysis of a given system, the Koopman eigenvalues($\mu_k$) and eigenfunctions ($\psi_k$) which capture the long term dynamics of the observables and the Koopman modes ($\nu_k$) which are vectors that allows us to reconstruct the system's state as a linear combination of the Koopman eigenfunctions.

### 2.2.1 Examples of Koopman Embeddings

In this section we will consider a simple example system containing a fixed point and possessing a closed form solution, as seen in [11, 27]:

$$\dot{\mathbf{x}}_1 = \mu x_1 \tag{2.10}$$

$$\dot{\mathbf{x}}_2 = \lambda(x_2 - x_1^2) \tag{2.11}$$

In 2.10 we have decoupled state with the absence of $x_2$ thus showing a linear equation. In 2.11 we see a squared term and non linearity. Here we notice that if $\lambda < \mu < 0$ then $x_2$ will rapidly approach $x_1^2$ showing a slow manifold approaching zero in a quadratic fashion with initial conditions aligning with the manifold and approaching zero showing the stability of the new system.

We can then augment the state by introducing a new term, an observable, $x_3 = x^2$ as a third state and thus making a linear system. Using the augmented state we can redefine the system linearly as:

$$\frac{d}{dt}\begin{bmatrix} y_1 \\ y_2 \\ y_3 \end{bmatrix} = \begin{bmatrix} \mu & 0 & 0 \\ 0 & \lambda & -\lambda \\ 0 & 0 & 2\mu \end{bmatrix} \begin{bmatrix} y_1 \\ y_2 \\ y_3 \end{bmatrix}, \tag{2.12}$$

with the new state space as:

$$\begin{bmatrix} y_1 \\ y_2 \\ y_3 \end{bmatrix} = \begin{bmatrix} x_1 \\ x_2 \\ x_1^2 \end{bmatrix}. \tag{2.13}$$

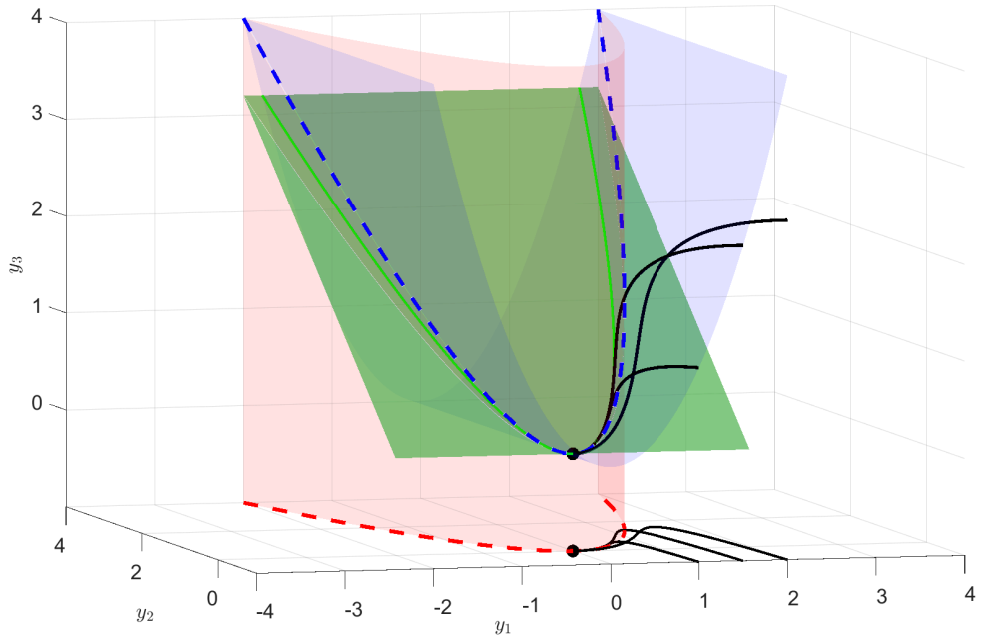


Figure 2.2: Three-dimensional Koopman system, linearized from 2.12 with dynamics projected onto the $y_1 - y_2$ plane. In red is the attracting slow manifold constrained by $y_3 = y1^2$ in blue and the unstable subspace described in 2.12 is the green plane. The trajectories of the linear Koopman system in $y$ are projected back onto the full nonlinear system states in $x$ in the $y_1 - y_2$ plane in black. In this example $\mu = -0.5$ and $\lambda = -5$. Reproduced from Brunton et al. [27]

By adding $y_3 = x^2$ in 2.12 we make 2.11 a linear equation. The third row simply is the derivative of $y_3$ which is $2\dot{x_1}x_1$ which in 2.13 is $\dot{x_1} = \mu x_1$ therefore making $\dot{y_3} = 2\mu x_1^2 = 2\mu y_3$. Thus this augmented state space of 2.10 and 2.11 and lifted to a three-dimensional Koopman observable space in 2.12 shown in Fig.2.2 via a new linear operator.

This does not work in all cases, if we were to take another simple non linear system such

as:

$$\frac{d}{dt}x = x^2 \rightarrow \begin{bmatrix} y_1 \\ y_2 \end{bmatrix} = \begin{bmatrix} x \\ x^2 \end{bmatrix}. \tag{2.14}$$

This should be a simple solution as it goes to infinity in a finite time, if we take the derivative of the second state we end up with:

$$\frac{d}{dt}y_2 = 2x\dot{x} = 2x^3. \tag{2.15}$$

As we can see $x^3$ is not contained within the original state space so continuing the method above we will never come to a closed solution and end up with an infinite amount of states and will need to rely on a Taylor expansion to solve it.

## 2.3 Dynamic Mode Decomposition

DMD is a data-driven method of exploring the behavior of complex systems. Using measurements from numerical simulations or in experiments, we can attempt to find the most dominant dynamic characteristics of the system. DMD does this by finding the dynamic modes or eigen modes and eigenvalues of the proposed system.
DMD acts on the assumption that the state of a system is connected to the next by

$$\mathbf{x}_{k+1} = \mathbf{A}\mathbf{x}_k, \tag{2.16}$$

where $\mathbf{x}(t) \in \mathbb{R}^n$ and $A \in \mathbb{R}^{n\times n}$ and is the matrix describing the evolution of the state in a continuous-time manner. Simulated or experimental measurements for $\mathbf{x}_k$ are then collected at regular time intervals of $\Delta t$ to become snapshots to be used in a discrete time system. These snapshots are collected and stored in sequence like the following:

$$\mathbf{X} = \begin{bmatrix} | & | & & | \\ \mathbf{x}_1 & \mathbf{x}_2 & \dots & \mathbf{x}_{m-1} \\ | & | & & | \end{bmatrix}, \tag{2.17}$$

$$\mathbf{X}' = \begin{bmatrix} | & | & & | \\ \mathbf{x}_2 & \mathbf{x}_3 & \dots & \mathbf{x}_m \\ | & | & & | \end{bmatrix}, \tag{2.18}$$

where $\mathbf{X}'$ is the time-shifted snapshot of matrix $\mathbf{X}$ such that

$$\mathbf{X}' \approx \mathbf{A}\mathbf{X}. \tag{2.19}$$

Mathematically, $\mathbf{A}$ is an operator that maps (2.17) onto (2.18) in a manner such that:

$$\mathbf{A}_{\mathbf{X}} = \underset{\mathbf{A}_{\mathbf{X}}}{\operatorname{argmin}} \|\mathbf{X}' - \mathbf{A}_{\mathbf{X}}\mathbf{X}\| = \mathbf{X}'\mathbf{X}^{+}. \tag{2.20}$$

There is no set number of snapshots required for DMD but a sufficiently large number is needed for the application and is closely related to the approximation of the Koopman operator. For DMD we are attempting to find the $\mathbf{A}$ in (2.19) using the snapshots of the system's states. $\mathbf{A}$ can be approximated by

$$\mathbf{A} = \mathbf{X}'\mathbf{X}^{+}, \tag{2.21}$$

where $^{+}$ is the Moore-Penrose pseudoinverse. Considering that $A$ has a large $n$ that normal calculation would be a large computational load we can perform singular value decomposition (SVD) on the snapshots to find the dominant characteristics of the pseudoinverse of $\mathbf{X}$

$$\mathbf{X} \approx \mathbf{U}\mathbf{\Sigma}\mathbf{V}^{*}, \tag{2.22}$$

where $\mathbf{U} \in \mathbb{R}^{n\times r}$, $\mathbf{\Sigma} \in \mathbb{R}^{r\times r}$ and $\mathbf{V} \in \mathbb{R}^{n\times r}$ where $*$ denotes the conjugate transpose. $r$ is the reduced rank of the SVD approximation of $\mathbf{X}$. From SVD we can rearrange the singular values and the eigenvectors of $\mathbf{X}$ with the forward snapshot to $A$ that satisfies (2.19):

$$\mathbf{A} \approx \tilde{\mathbf{A}} = \mathbf{X}'\tilde{\mathbf{V}}\tilde{\mathbf{\Sigma}}^{-1}\tilde{\mathbf{U}}^{*}, \tag{2.23}$$

where $\tilde{A}, \tilde{V}, \tilde{\Sigma}$ and $\tilde{U}^{*}$ is an approximation of $A, V, \Sigma$ and $U$, seen in (2.22) based on the truncation rank $r$.

However, since we primarily care about the $r$ leading eigenvectors and eigenvalues of $\mathbf{A}$, we can project $\mathbf{A}$ onto the modes of $\mathbf{U}$ such that:

$$\tilde{\mathbf{A}} = \mathbf{U}^{*}\mathbf{X}'V\mathbf{\Sigma}^{-1}, \tag{2.24}$$

where $\tilde{A}$ linear model of the dynamical system such that

$$\tilde{\mathbf{x}}_{k+1} = \tilde{\mathbf{A}}\tilde{\mathbf{x}}_k. \tag{2.25}$$

Here $\tilde{\mathbf{x}} :\in \mathbb{R}^{r\times 1}$ is also a reduced order of the state $\mathbf{x}$ which can be reconstructed by

$$\tilde{\mathbf{x}} : \mathbf{x} = \tilde{\mathbf{U}}\tilde{\mathbf{x}}. \tag{2.26}$$

The next step is to find the spectral decomposition of $\tilde{\mathbf{A}}$:

$$\tilde{\mathbf{A}}\mathbf{W} = \mathbf{W}\mathbf{\Lambda}, \tag{2.27}$$

where $\mathbf{\Lambda}$ and $\mathbf{W}$ are the corresponding eigenvalues (DMD modes) and eigenvectors of the full rank system dynamics matrix allowing us to recover the full state system dynamics in a computationally efficient manner since $\tilde{\mathbf{A}} \in \mathbb{R}^{r\times r}$ where $r << n$. We can now reconstruct the eigendecomposition in (2.22) for $\mathbf{A}$ from $\mathbf{W}$ and $\mathbf{\Lambda}$ with the corresponding eigen vectors given by the columns of $\mathbf{\Phi}$ such that

$$\mathbf{\Phi} = \mathbf{X}'\mathbf{V}\mathbf{\Sigma}^{-1}\mathbf{W}. \tag{2.28}$$

From $\mathbf{\Phi}$ we can no reconstruct our approximation of the time dynamics of $\mathbf{x}(t)$ by projecting our approximations into a future solution

$$\mathbf{x}(t) \approx \sum_{k=1}^{r} \boldsymbol{\phi}_k \exp(\omega_k t) b_k = \mathbf{\Phi} \exp(\mathbf{\Omega} t) b, \tag{2.29}$$

where $b_k$ is the initial amplitude of each DMD mode, $\boldsymbol{\phi}$ is the columns that make up $\mathbf{\Phi}$ and $\mathbf{\Omega}$ is the diagonal matrix of the eigenvalues $\omega$ in $\omega_k = \ln(\lambda_k)/\Delta t$ [9, 11, 14, 26, 30].

## 2.4 Finding the Koopman Operator with Dynamic Mode Decomposition: Extended DMD

Extended DMD (EDMD) is almost the same algorithm as the standard DMD one, however the method of which we deploy EDMD is by using the observables of the system to create a dictionary to pass through the normal DMD algorithm. By performing regression on this new augmented vector containing linear and non-linear measurements we can make a different

approximation of the original system dynamics. This augmented vector is constructed in the following manner:

$$y = \Theta^T(\mathbf{x}) = \begin{bmatrix} \theta_1(\mathbf{x}) \\ \theta_2(\mathbf{x}) \\ \vdots \\ \theta_p(\mathbf{x}) \end{bmatrix}. \tag{2.30}$$

where $p$ is the rank of the augmented state such that $p >> n$. Here $\Theta$ is the collection of measurements of the system possibly containing the original state of the system, $\mathbf{x}$, as well as nonlinear measurements. Once $y$ is found, two data matrices are created in the same manner seen above in the DMD algorithm (2.17)(2.18).

$$\mathbf{Y} = \begin{bmatrix} | & | & & | \\ \mathbf{y}_1 & \mathbf{y}_2 & \cdots & \mathbf{y}_{m-1} \\ | & | & & | \end{bmatrix}, \tag{2.31}$$

$$\mathbf{Y}' = \begin{bmatrix} | & | & & | \\ \mathbf{y}_2 & \mathbf{y}_3 & \cdots & \mathbf{y}_m \\ | & | & & | \end{bmatrix}, \tag{2.32}$$

From here a best-fit linear operator $A_Y$ is found that maps a set of snapshots of (2.30) developed in the same manner as (2.17) and (2.18)

$$\mathbf{A_Y} = \underset{\mathbf{A_Y}}{\operatorname{argmin}} \|\mathbf{Y}' - \mathbf{A_Y}\mathbf{Y}\| = \mathbf{Y}'\mathbf{Y}^+ \tag{2.33}$$

This regression can than be written in terms of the original data matrices $\Theta^T(\mathbf{x})$

$$\mathbf{A_Y} = \underset{\mathbf{A_Y}}{\operatorname{argmin}} \left\|\mathbf{\Theta^T}(\mathbf{x}') - \mathbf{A_Y}\mathbf{\Theta^T}(\mathbf{x})\right\| = \mathbf{\Theta^T}(\mathbf{x}')(\mathbf{\Theta^T}(\mathbf{x}))^+. \tag{2.34}$$

$A_X$ is then the basis upon which we can derive the Koopman operator. However, $\Theta$ may not necessarily span the same subspace as the Koopman operator and may consist of different eigenvalues and eigenvectors of the Koopman operator when is why verification and re-validation techniques need to be used to show that the EDMD model is properly fit to the actual system.

### 2.4.1 Choice of Dictionary

As mentioned previously, we augment the state space of a system when determining the Koopman operator using EDMD. We discussed one method of augmenting the system by taking the Jacobian of the original space in section 2.1.1 and how this method of lifting the state space is not always applicable. For systems with out a closed solution, other dictionaries can be used to find a more appropriate solution. A dictionary in this application is a specific method which we use to augment a state space to cause the eigen values and eigen modes of the state space to form a closed form solution. These dictionaries are usually system specific [10,16,19,23] as seen in these works however there are several generic ones that we will discuss here.

In [10]and [19] the authors explored lifiting a duffing oscillator and a cart-pendulum like system using a combination of polynomial and Fourier basis' as there dictionaries. In [19] when searching for optimal control, they lifted the control data with the state-space to further the lifting process and found that low orders had marginal affects on the reconstruction of the state data before EDMD could no longer capture and reconstruct the original dynamics. Traditionally a polynomial basis function lifts the original state space as:

$$y_i(x) = x_1^{\alpha_i} x_2^{\beta_i} ... x_n^{\delta_i}, \tag{2.35}$$

where $\alpha, \beta, \delta$ are non negative integers corresponding to the order in which the polynomial basis is performed and $i$ is the $i^{th}$ state of the original system. For a Fourier basis lifting function, in this work we will be using:

$$y_i(x) = \prod_{x_i} \prod_{k_j} \cos(k_j x_i) \sin(k_j x_i), \tag{2.36}$$

where $k_j$ i s the $j^{th}$ basis order such that $\Sigma_j k_j < Q$ where $Q$ is the largest basis degree in the set.

In [16], Williams et al. describe thee other simple lifting functions that have shown to be successful in finding the Koopman operator through EDMD in other systems. These dictionaries are lifting using Hermite polynomials, radial basis functions and discontinuous spectral elements. Using Hermite polynomials as a lifting function works best for states are are defined on $\mathbb{R}^n$ when the data is normally distributed (not in a stochastic sense). This is very similar to the polynomial basis function described above. Using a radial basis function is best used for problems defined on irregular domains such as problems with complex geometries

and mesh grids can be difficult to compute. Lastly, using discontinuous spectral elements are best used for problems where blocks of data can be isolated and lifted individually using their own basis functions, essentially decoupled.

### 2.4.2 Limitations Koopman Operator and DMD

There are several weaknesses with the Koopman operator as it is not a solution to every dynamical system. The first major weakness of the Koopman operator especially with respect to DMD, is the need for sufficient data. This sufficiency is both dependent on states sampled if the system in question has coupled states which are of importance to us, and in terms of time steps as we increase the number of snapshots when performing DMD we get a clearer image of the underlying dynamics [9, 11].

Another principle weakness of the Koopman operator is that it is system specific and depending on which method you use to identify the Koopman operator from data you will be limited to a set course of dynamics that the system would expect to experience. Another way to state this is that the Koopman operator for one set of maneuvers is not guaranteed to work on another set of maneuvers of the same dynamical system. Other weaknesses of the Koopman operator is that the Koopman modes may not exist or be insignificant at all times in a given span. Likewise it is also possible that a single Koopman mode may be associated with multiple Koopman eigen values as we will show later in this work [6, 9, 11].

Additionally, there is a need for clarity in the observations taken when forming the Koopman operator from data. As discussed in [22, 23] the need to filter the data used may be required to find the Koopman operator of the underlying system. Additionally since the Koopman operator is derived form the eigenfunctions and eigen modes of the system, noisy data can cause DMD to find dominate modes in the data where there are peaks in the measurement noise.

## 2.5 Methodology

### 2.5.1 Approximating Koopman Eigenfunctions from Data

Beginning with the observable matrices in (2.30), the Koopman eigenfunction can be approximated as

$$\varphi(\mathbf{x}) \approx \sum_{k=1}^{p} \boldsymbol{\theta}_k(\mathbf{x})\boldsymbol{\xi}_k = \boldsymbol{\Theta}(\mathbf{x})\boldsymbol{\xi}, \tag{2.37}$$

where by using (2.30), we can find

$$\begin{bmatrix} \lambda\varphi(\mathbf{x}_1) \\ \lambda\varphi(\mathbf{x}_2) \\ \vdots \\ \lambda\varphi(\mathbf{x}_m) \end{bmatrix} = \begin{bmatrix} \varphi(\mathbf{x}_2) \\ \varphi(\mathbf{x}_3) \\ \vdots \\ \varphi(\mathbf{x}_{m+1}) \end{bmatrix}. \tag{2.38}$$

We start seeing a connection between the Koopman operator and the process we followed to approximate a linear evolution seen in DMD. We can expand (2.37) as

$$[\lambda\boldsymbol{\Theta}(\mathbf{X}) - \boldsymbol{\Theta}(\mathbf{X}')]\boldsymbol{\xi} = 0. \tag{2.39}$$

Afterwards, we reduce (2.39) using a best least-squares fit to get

$$\lambda\boldsymbol{\xi} = \boldsymbol{\Theta}(\mathbf{X})^{+}\boldsymbol{\Theta}(\mathbf{X}')\boldsymbol{\xi}. \tag{2.40}$$

Now we can compare (2.34) and (2.40); (2.34) is the transpose of the latter so that the left eigenvectors are now the right eigenvectors. Comparing to (2.21) we can use the eigenvectors $\boldsymbol{\xi}$ of $\boldsymbol{\Theta}^{+}\boldsymbol{\Theta}'$ to find the coefficients of the eigenfunction $\varphi(\mathbf{x})$ that represents the basis of $\boldsymbol{\Theta}(\mathbf{x})$. We now can confirm that the predicted eigenfunctions behave linearly by comparing them to the predicted dynamics in (2.38). We do this to determine if the regression done in (2.40) yields proper eigenvalues and eigenvectors that span the Koopman invariant subspace for the system [16].

# CHAPTER 3
# IMPLEMENTATION OF KOOPMAN OPERATOR ON SAMPLE SYSTEMS

In this chapter we will discus the two systems we used DMD and EDMD to find the Koopman operator for and how we generated the data and the boundaries in which we analyzed the effectiveness these algorithms had at finding a usable Koopman Operator. In this section we will be using data sets from a controlled and uncontrolled pendulum and cart-pole system and change the sampling rate and sample duration in which we used to calculate the respective Koopman operators. Additionally we tested the fidelity of the reconstructions of EDMD through a combination of polynomial and Fourier basis functions and the effectiveness each had in reconstructing the data. Lastly we explored the effects of truncation when reconstructing the EDMD data and the accuracy of these reconstructions.

## 3.1 Sample Systems

The classical systems that were used in this work to approximate the Koopman operator are the inverted pendulum and cart pole system. These systems are used due to their periodic and transient behaviors and dynamics are well known. The pendulum is a good candidate system since it has a periodic behavior which can be easily captured through DMD/EDMD. The cart-pole system builds onto the pendulum by including an additional degree of freedom to the system, horizontal movement on a rail. In this work, we looked at both these systems with the swinging mass in the inverted position and undamped.

### 3.1.1 Defining the Inverted Pendulum

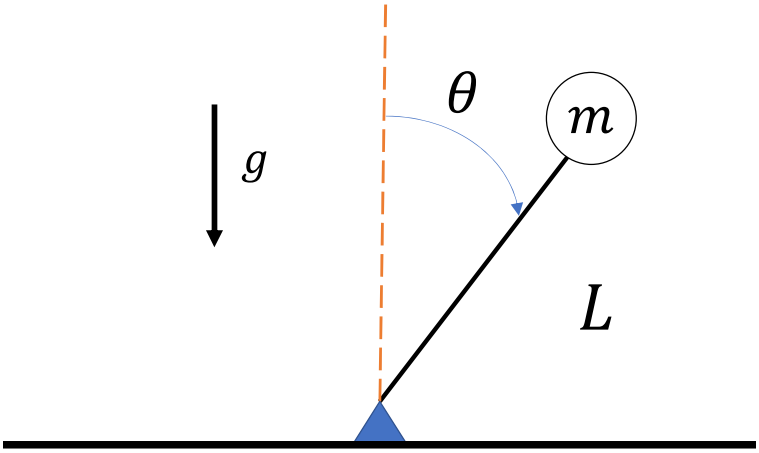


Figure 3.1: Classical inverted pendulum system with mass $m = 1.0\ kg$ and arm length of $L = 2.0\ m$. In this model the mass is free to swing about the pivot 360 degrees and will be treated as an undamped system.

For this work the first system we looked at is a simple pendulum in an inverted position as seen in Fig. 3.1. The dynamics we used for this work are [12]:

$$\dot{\mathbf{x}} = \begin{bmatrix} \dot{\mathbf{x}}_1 \\ \dot{\mathbf{x}}_2 \end{bmatrix} = \frac{d}{dt} \begin{bmatrix} \theta \\ \dot{\theta} \end{bmatrix} = \begin{bmatrix} \dot{\theta} \\ \frac{g}{L} \sin\theta \end{bmatrix} + \begin{bmatrix} 0 \\ \frac{1}{mL^2} \end{bmatrix} u, \tag{3.1}$$

where the mass at the end of the pendulum, $m$ is 1.0 $kg$ for all simulations and has an a massless, rigid arm with length $L = 2.0\ m$. In all simulations in this work, $g$ is the gravitational acceleration with an assumed value of 9.81 $m/s^2$. This pendulum is free to rotate 360 degrees and has a frictionless pivot.

For all pendulum simulation setups, we will start with an initial state of $[\pi/4, 0]$ unless otherwise stated, and in the controlled examples we attempted to right the pendulum mass to a terminal state of $[0, 0]$. For this sample system and for the cart-pole system we will be using a linear quadratic regulator (LQR) to determine the optimal gain to stabilize the systems to their final states. In this simulation we only controlled the $\dot{\theta}$ term with a performance index of $[0, 10]$ and a control cost of 10 for our optimal gain found through using LQR. When calculating the LQR gain for this system we used the following models for the linearized

$\mathbf{A}_{pend}$ and $\mathbf{B}_{pend}$ matrices:

$$\mathbf{A}_{pend} = \begin{bmatrix} 0 & 1 \\ -L/g & 0 \end{bmatrix} \tag{3.2}$$

$$\mathbf{B}_{pend} = \begin{bmatrix} 0 \\ 1 \end{bmatrix}. \tag{3.3}$$

### 3.1.2 Defining the Cart-Pole

The second system that we will analyze in this work is the classical cart-pole system. The nonlinear dynamics we used for this work are given as [11]:

$$\dot{\mathbf{x}} = \begin{bmatrix} \dot{x_1} \\ \dot{x_2} \\ \dot{x_3} \\ \dot{x_4} \end{bmatrix} = \frac{d}{dt} \begin{bmatrix} x \\ \dot{x} \\ \theta \\ \dot{\theta} \end{bmatrix} = \begin{bmatrix} \dot{x} \\ \dfrac{-m^2L^2g\cos\theta\sin\theta + mL^2(mL\dot{\theta}^2\sin\theta + mL^2u}{mL^2(M + m(1-\cos\theta^2)} \\ \dot{\theta} \\ \dfrac{(M+m)mgL\sin\theta - ml\cos\theta(mL\dot{\theta}^2\sin\theta) + ml\cos\theta u}{mL^2(M + m(1-\cos\theta^2)}. \end{bmatrix} \tag{3.4}$$

where $x$ is the position of the cart on the track, $\dot{x}$ is the velocity of the cart down the track, $\theta$ is the angle of the weighted mass arm from the center of the cart and $\dot{\theta}$ is the rotational rate of the arm. $M$ is the cart mass where in this simulation is 5 $kg$, $m$ is the pendulum mass ($m = 1.0\ kg$), $L$ is the arm pendulum arm length ($L = 2\ m$). As aforementioned, this system will be treated as undamped and frictionless about the track the cart is resting on and about the pivot arm which is allowed to rotation about its pivot 360 degrees as seen in Fig. 3.2.

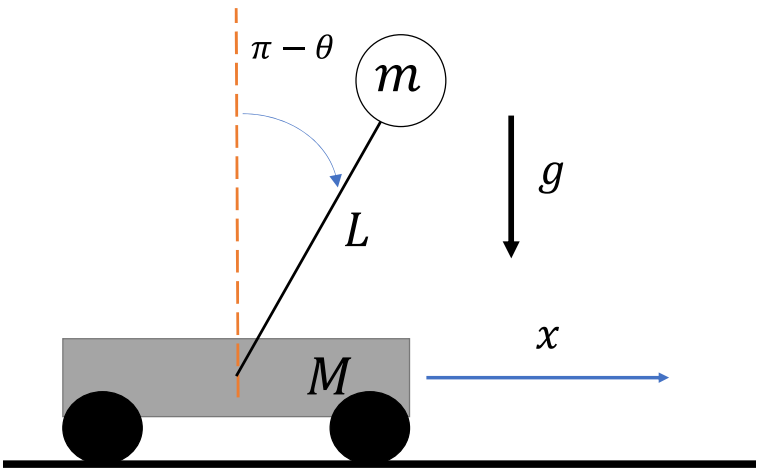


Figure 3.2: Classical cart pole system with pendulum mass $m = 1.0\ kg$, cart mass $M = 5.0\ Kg$, and arm length $L = 2\ m$. Like the pendulum system in Fig. 3.1, the end mass is free to swing about the pivot 360 degrees and both the cart and arm pivot are friction-less and undamped.

For respective simulations, this system started with an initial state of $[-1, 0, \pi, 0]$ and when controlled, attempted to right the cart-pole system after a brief translation to $[1, 0, \pi, 0]$. Similar to the previous system, the controlled data will be generated using LQR to determine an optimal gain with a performance index of $[5, 10, 0, 5]$ and a control cost of 10. When calculating the optimal gain using LQR we used the following models for the linearized $\mathbf{A}_{cart}$ and $\mathbf{B}_{cart}$ matrices:

$$\mathbf{A}_{cart} = \begin{bmatrix} 0 & 1 & 0 & 0 \\ 0 & -1/M & gm/M & 0 \\ 0 & 0 & 0 & 1 \\ 0 & -1/(ML) & -g(M+m)/(ML) & 0 \end{bmatrix} \tag{3.5}$$

$$\mathbf{B}_{cart} = \begin{bmatrix} 0 \\ 1/M \\ 0 \\ 1/(ML) \end{bmatrix}. \tag{3.6}$$

## 3.2 Discovering the Koopman Operator for a Pendulum System

### 3.2.1 Koopman Reconstruction of a Pendulum using DMD

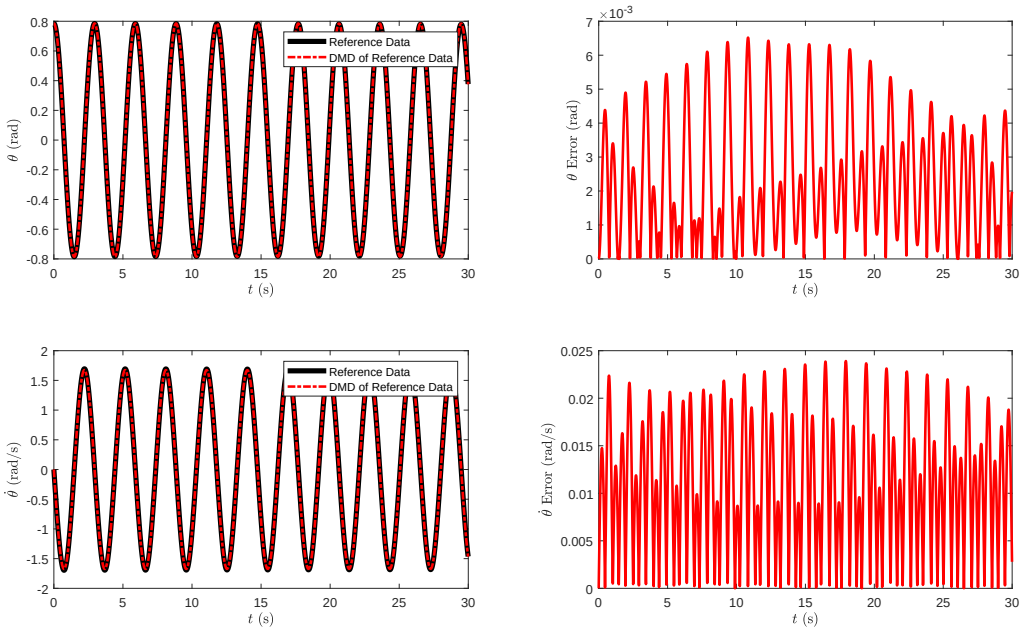


Figure 3.3: DMD performed on an uncontrolled pendulum system over a period of 30 seconds and at a 100 Hz sampling rate and the reconstruction error associated with each state.

In Fig. 3.3 we took the nonlinear states of an uncontrolled pendulum system over a span of 30 seconds and a 100 Hz sampling rate with the initial conditions described in subsection 3.1.1 and using the method described in section 2.3 to find the Koopman operator and reconstruct the system from the data. This full state reconstruction a high fidelity reconstruction of the original state data with low error showing the strengths of DMD on dynamical systems with cyclic behavior.

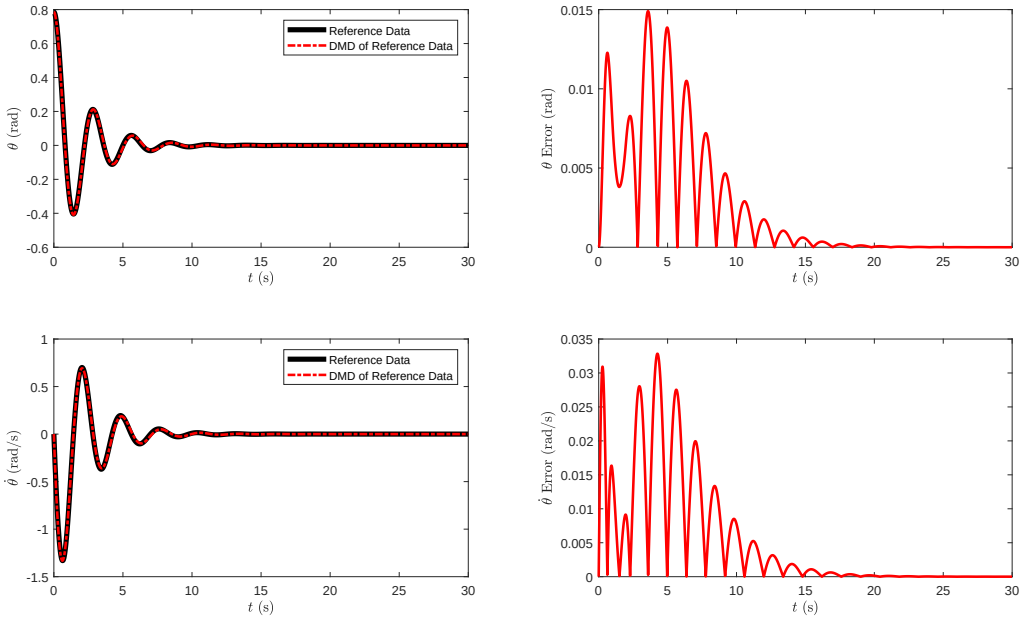


Figure 3.4: DMD performed on a pendulum system with with a LQR controlled data over a period of 30 seconds and at a 100 Hz sampling rate and the reconstruction error associated with each state.

In Fig. 3.4 we took the numerical solution to the nonlinear states of a pendulum system with the same boundary conditions as above that is stabilized in the upright position with a LQR controller. While there are higher peaks in the error for the controlled data we can still recreate a high fidelity full state reconstruction using DMD. The cyclic inherent behavior of the pendulum system is still observed and pronounced in this reconstruction towards the end of the simulation duration but still remains faithful to the original data set.

### 3.2.2 Koopman Reconstruction of a Pendulum using EDMD

Additionally, we explored different, low order combinations using polynomial and Fourier series basis'. In this study we limited the lifting function combinations to a second order polynomial basis, a second order polynomial basis with a first order Fourier series basis, a first order Fourier series basis alone, and a second order Fourier basis. We can see here that the reconstruction using the Fourier series as a lifting function yields the highest fidelity models for the uncontrolled pendulum simulation data as seen in Fig. 3.5.

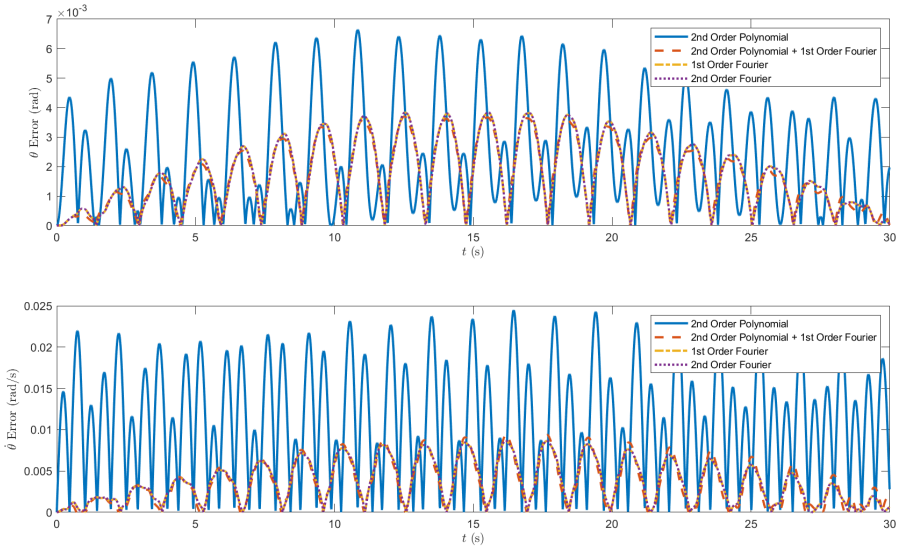


Figure 3.5: State error for four combinations of lifting for EDMD on the pendulum system on the uncontrolled data set.

In Fig. 3.6 we tested the four different lifting function combination on the controlled pendulum data. The reconstruction of the controlled states shows a similar difference in reconstruction accuracy as seen in Fig. 3.5 though the reconstructions have noticeable differences in their accuracy. While the Fourier series combinations have lower errors, the second order Fourier basis noticeably has the lowest reconstruction error. The EDMD reconstructions show a persisting periodic behavior in the reconstruction that is not present in the reference data showing how DMD/EDMD maintains the initial dynamics of the reference data throughout the reconstruction of the state data.

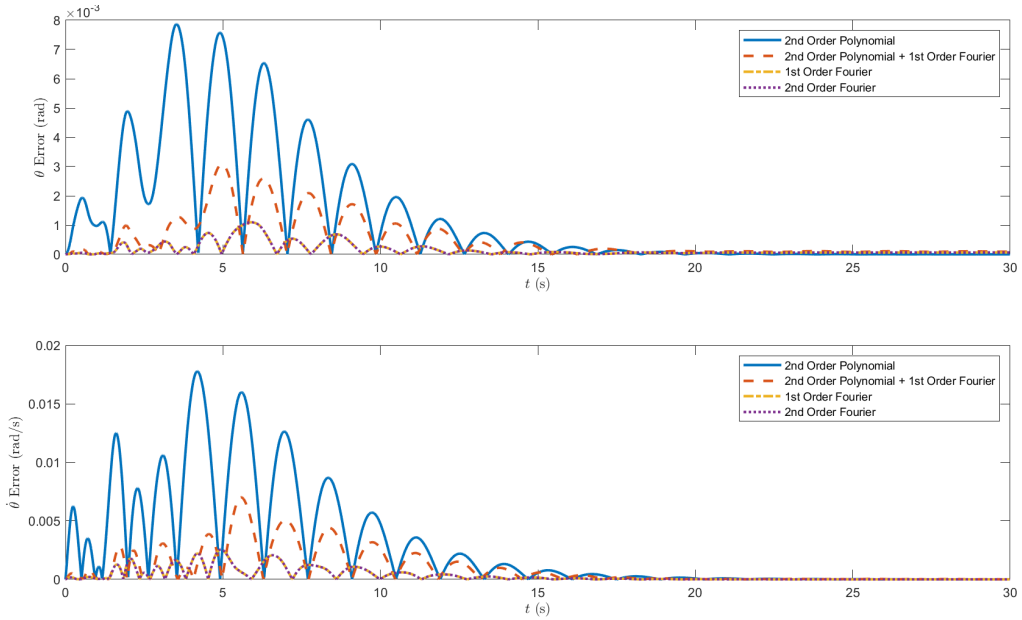


Figure 3.6: State error for four combinations of lifting for EDMD on the pendulum system on the controlled data set.

## 3.3 Discovering the Koopman Operator for a Cart-Pole System

### 3.3.1 Koopman Reconstruction of a cart-pole using DMD

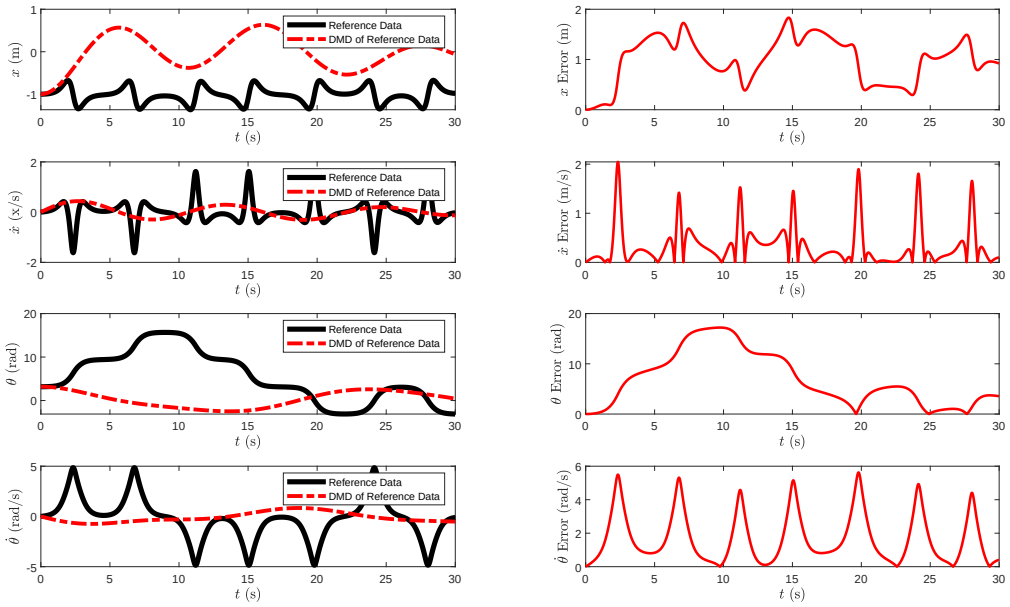


Figure 3.7: DMD performed on a cart-pole system with uncontrolled data over a period of 30 seconds and a 1 ms sampling rate.

In Fig. 3.7 we took the nonlinear states of a cart-pole system over a span of 30 seconds and a 100 Hz sampling rate with the initial conditions described in subsection 3.1.2 and using the method described in section 2.3 to find the Koopman operator and reconstruct the system from the data. Unlike the pendulum model, the uncontrolled data set was not accurately captured or reconstructed using DMD. This is likely due to the change in the system dynamics when the pendulum mass falls below the cart track. While the $\theta$ state can be corrected to fall within a 0 to $2\pi$ range, the reconstructed dynamics do not improve. Additionally due to the non-periodic behavior seen in the two transient states of the cart pole in this simulation the eigen modes found in DMD appear to be significantly damped during the reconstruction.

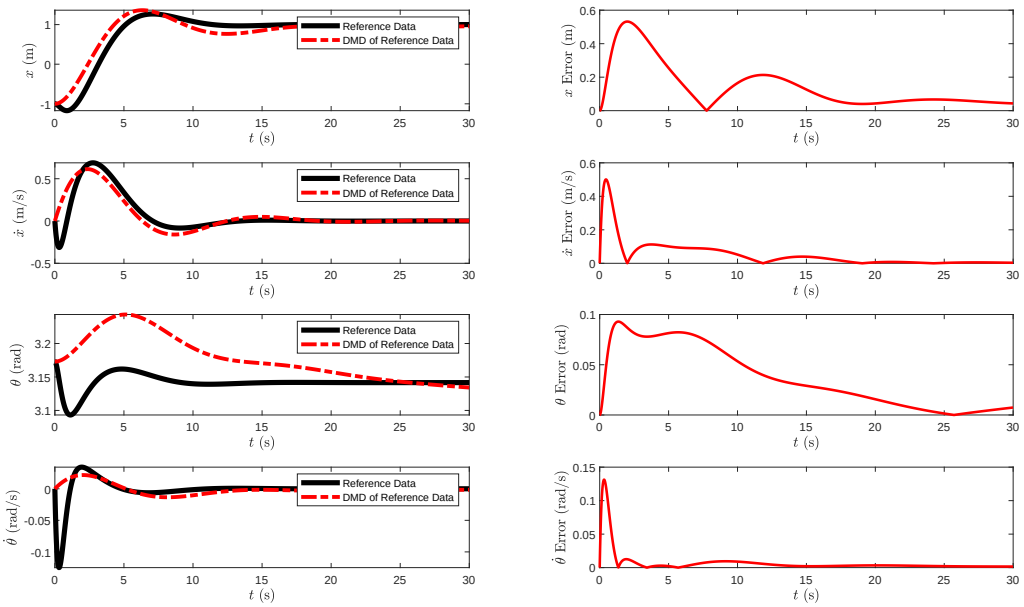


Figure 3.8: DMD performed on a cart-pole system with with a LQR controlled data over a period of 30 seconds and a 1 ms sampling rate.

In Fig. 3.8 we took the numerical solution to the nonlinear states of a cart-pole system with the same boundary conditions as above that is stabilized in the upright position, 1 $m$ to the right of the initial position with a LQR controller. While less accurate than the pendulum model, the controlled data appears to be captured in three of the four states using EDMD. The $\theta$ state appears to be missed and some of the initial control peaks appear to be missed in the data reconstruction. This may be due to the lack of a periodic behavior that would be seen in the $x$ and $\dot{x}$ states of the cart pendulum system and the Koopman eigenfucntions and modes cannot discern between the still periodic nature of the $\theta$ and $\dot{\theta}$ states with the aforementioned ones.

### 3.3.2 Koopman Reconstruction of a cart-pole using EDMD

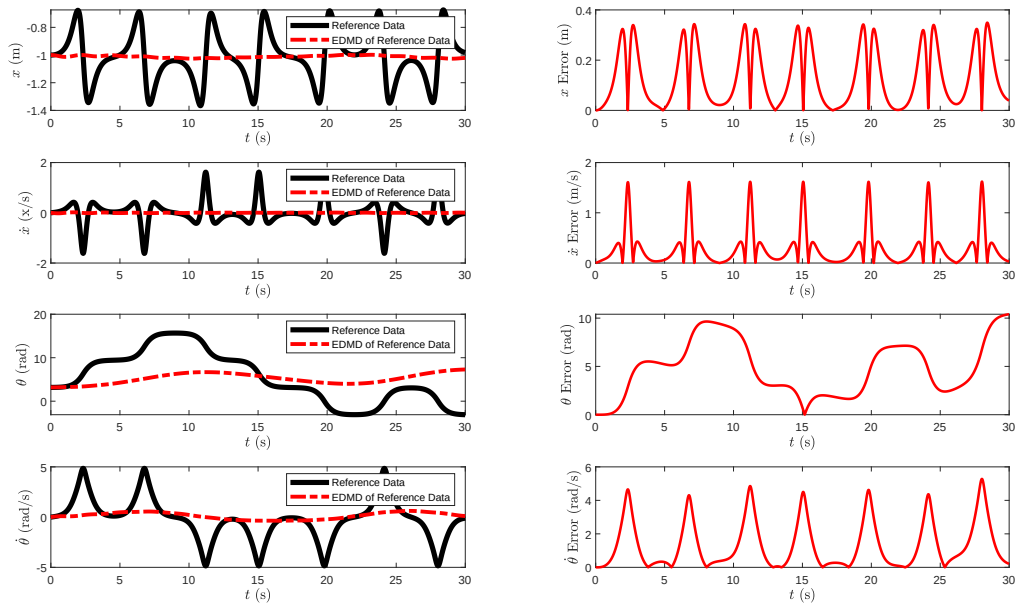


Figure 3.9: DMD performed on a cart-pole system with uncontrolled data over a period of 30 seconds and a 1 ms sampling rate.

In Fig. 3.9 we found the Koopman operator for the reference uncontrolled cart-pole data lifted with a second order polynomial basis function. Like the DMD reconstruction, the EDMD reconstruction fails to capture the dominant modes in the system dynamics of the uncontrolled system and like the DMD reconstruction, there was no noticeable improvement when the range of the $\theta$ term is restricted within the 0 to $2\pi$ range. A point of note is that the cart-pole EDMD reconstruction show in this figure does not capture any of the transient dynamics of the system.

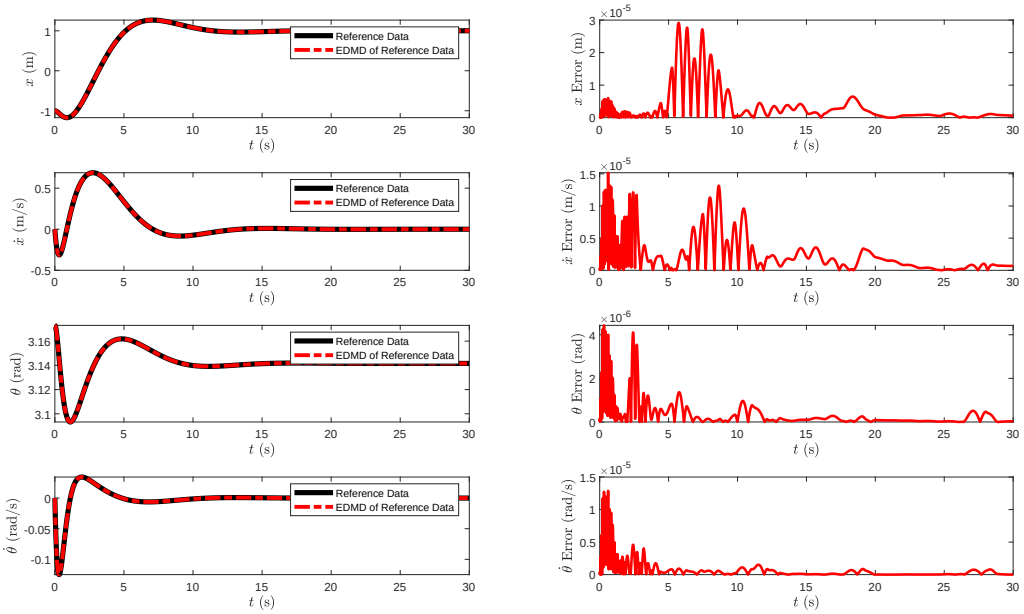


Figure 3.10: DMD performed on a cart-pole system with with a LQR controlled data over a period of 30 seconds and a 1ms sampling rate.

In Fig. 3.10 we found the Koopman operator for the reference controlled cart-pole data lifted with a second order polynomial basis function. Here we can see that there is a superior reconstruction of the controlled state compared to the DMD reconstruction. We can also see a small spike in the error for the EDMD reconstruction at the local maxima and minima which means that the magnitudes of the Koopman modes of the data are not properly being captured and may need to to have a shallower control input to more accurately capture the underlying dynamics of the controlled system.

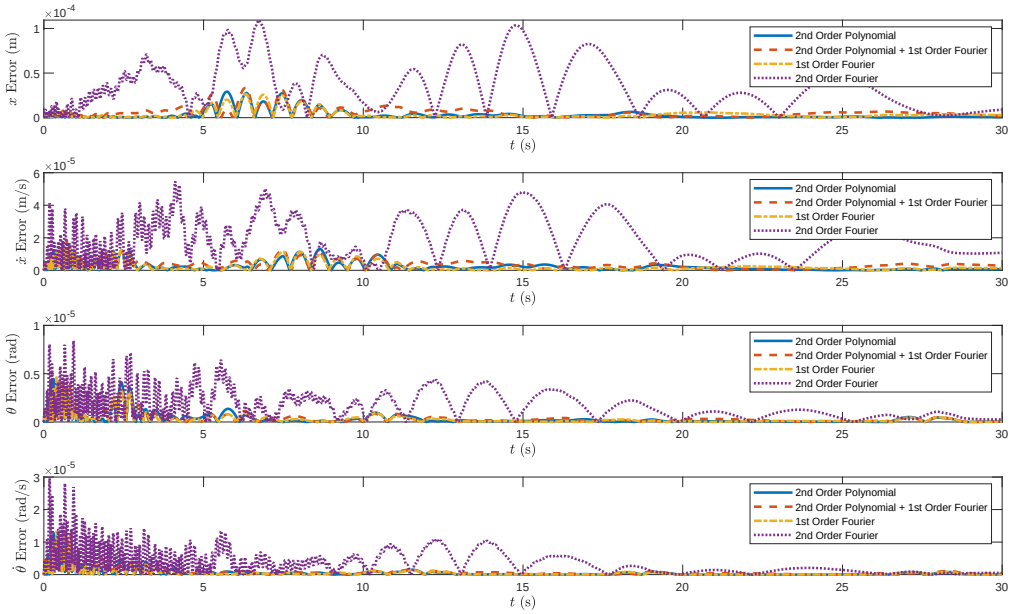


Figure 3.11: Four combinations of lifting for EDMD on the cart-pole system on the controlled data set.

In Fig. 3.11 we tested the four different lifting function combination on the controlled cart-pole data. We will only report on the controlled data set since as seen in the previous two subsections, the uncontrolled cart-pole data cannot be captured through DMD or EDMD. We can see here that unlike in the pendulum setup, the Fourier series is not noticeably more accurate with the second order Fourier basis being wildly less accurate showing stronger periodic behaviors not present in the initial data.

## 3.4 Effects of Truncation on EDMD Approximated Systems

In this section we will discuss the results of restricting the Koopman reconstruction of the two sample systems to the same number of states as the original system data set. This will be how we will truncate the the lifted states and if we were given the infinite dimensional data set that was part of the original theory behind the Koopman operator, this would be one of the ways we can bring it down to a finite number of states. As described in Section 2.3, equation 2.23 of the DMD decomposition and reconstruction process (this also applies to EDMD), the $r$ term can be reduced to some smaller value relating to the total number of

states that will be present in the eigen reconstruction. In [10,14] the authors truncated their system dynamics by the magnitude of their singular values found in the SVD process and in [25] the authors truncated their singular values using the optimal hard threshold algorithm described in [31]. While the rank that we will be truncating our approximated Koopman operator to is mathematically arbitrary, the novelty is to explore the incurred error and the effects it has on reconstruction.

### 3.4.1 Effects of Truncation on EDMD Reconstructed Pendulum Setup

In the previous subsections we discussed a full state reconstruction of the reference data we used in both the DMD and EDMD process. Since the ultimate goal of a Koopman approximation is to reduce the interdenominational Koopman subspace down to a finite number of dimensions we then truncated the lifted data down to the same number of states as the initial pendulum system.

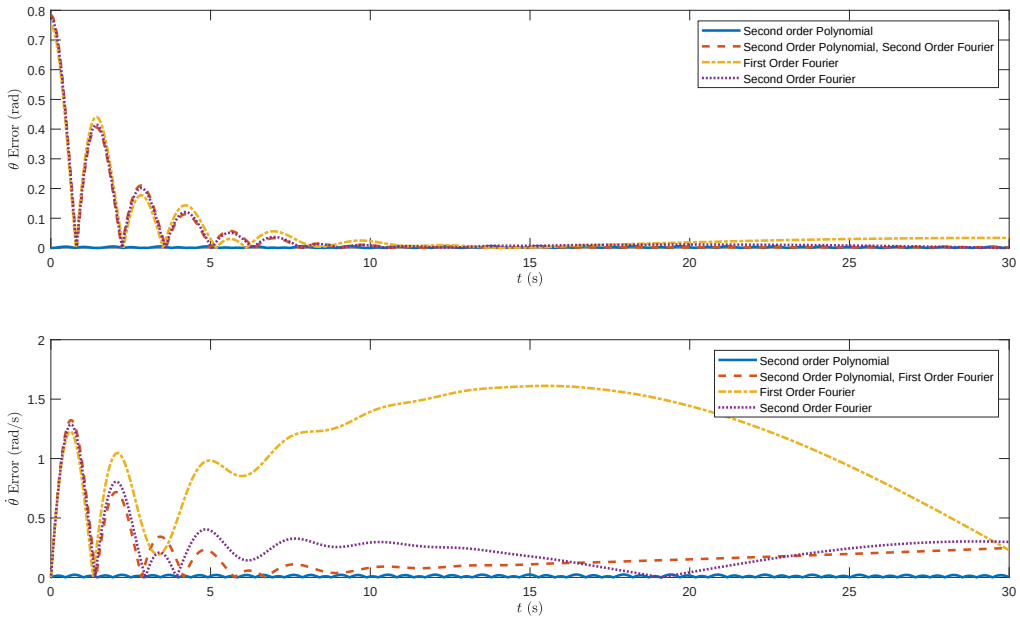


Figure 3.12: State error for four combinations of lifting for EDMD on the pendulum system on the uncontrolled data set. This reconstruction was limited to a two state solution using EDMD.

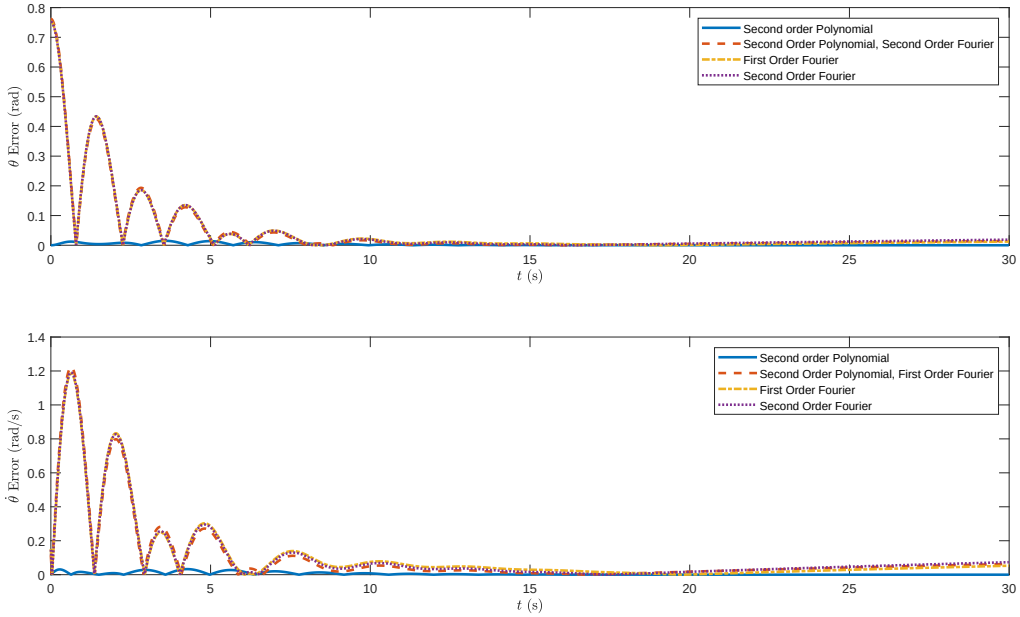


Figure 3.13: State error for four combinations of lifting for EDMD on the pendulum system on the controlled data set. This reconstruction was limited to a two state solution using EDMD.

We can see that there are significant differences between the truncated and full state reconstructions in Figs. 3.12 and 3.13. While the full state has more accurate reconstructions of the reference data lifted with a Fourier basis we can see the opposite is true for the truncated reconstruction. In Fig. 3.12 we can see that there were significant reconstruction errors with the uncontrolled $\dot{\theta}$ state data, predominantly within the first order Fourier basis. This error is also more pronounced in the other Fourier combinations showing that the Fourier basis provides stronger modes at higher dimensions than in the original data set and the reconstructed data using the second order polynomial lift. Additionally, due to the way the Fourier basis function would augment the original state space, when truncating down to a lower state it is possible that this process may inadvertently have removed a specific augmented state that is strongly coupled to the original states of the system and removing this state This is seen in the lower error of the polynomial and Fourier basis lift having less error than the data lifted solely through a Fourier basis.

### 3.4.2 Effects of Truncation on EDMD Reconstructed Cart-pole Setup

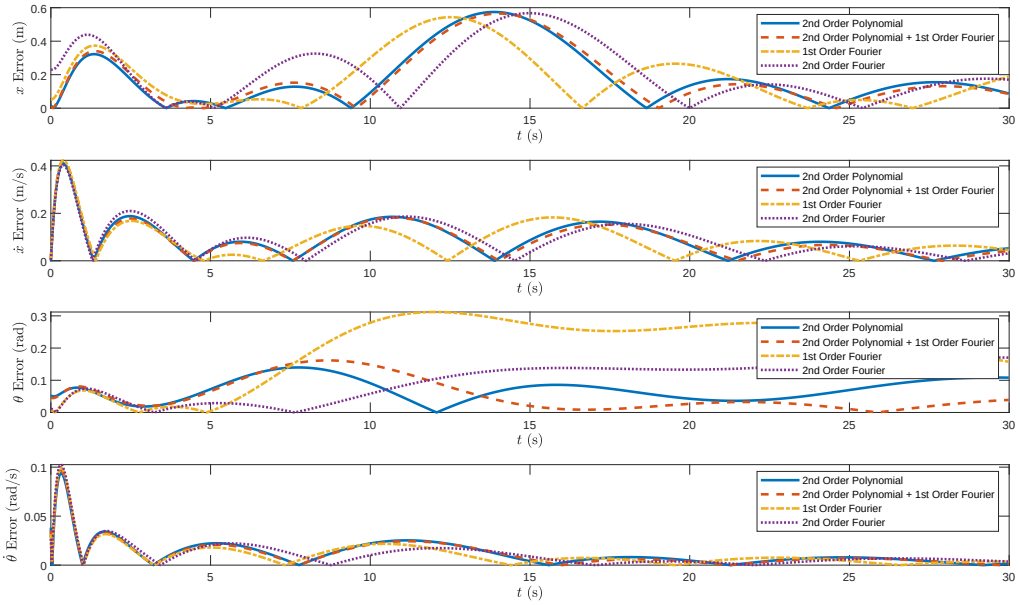


Figure 3.14: State error for four combinations of lifting for EDMD on the cart-pole system on the controlled data set. This reconstruction was limited to a four state solution using EDMD.

In Fig. 3.14 we tested the four different lifting function combination on the controlled cart-pole data using a truncated rank from EDMD. In these simulations we truncated the same lifted data in subsection 3.3.2 down to four states in the Koopman reconstruction. We can see here that the reconstructed data is far less varied than that of the full state EDMD reconstruction, most notably that the second order Fourier basis lift is less periodic in the reconstruction of the data. We can also see considerable losses in the first three state's reconstruction showing that all the dictionaries used to lift the original state space spread the dynamics more dominantly among the augmented states showing what appear to be transient, unbounded errors over a longer time span. Despite this, the truncated state has significantly more error than the full state reconstruction, in the $\dot{x}$ state's case there are over three orders of magnitude of difference in the reconstruction.

### 3.4.3 Analysis of Behavior on EDMD Truncation

As seen in Fig. 3.12 we can begin to see the effects of dropping dominant modes in the Koopman reconstruction. In the $\dot{\theta}$ error plot in this figure we can see the effects of what appear to be three unbounded errors relating to the lifting with the Fourier basis dictionary.

This was expected due to the removal of an arbitrary amount of less dominant modes that most likely corresponded to a set of dynamics that was expressed in following modes after the truncation cutoff. Due to the loss of these dynamics in the reconstruction, growing errors in the linearization prevailed during the reconstruction process. In Fig. 3.13 we can see some smaller errors forming at the end of the data set but if we were to continue plotting over a longer time span we would see that these errors appear to be bounded. This observation leads to believe that the dropped eigen mode describes the dynamics of a periodic nature that were brought about by either the initial dynamics in the normal state space or as a byproduct of the choice of lifting functions used. These are important factors to consider when choosing how to choose an $r$ when truncating during the Koopman reconstruction as when using these derived linear models for control application a periodic, bounded error may be neglected while an unbounded error can cause the reconstruction error and is a point of future analysis.

## 3.5 Effects of Variance in Data Collection

We also explored the effects of variance of the data used to find the Koopman operator in the two systems discussed above. In a practical application of the Koopman operator to model and eventually control a mechanical system an abundance of clean, high resolution data may not be available in all situations. To meet this challenge we Incorporated three variances to the data when running the simulations of the two pendulum systems. In this section we will discuss the results of increasing and decreasing the resolution via the sampling rate, decreasing the quantity of data by reducing the observation window down to 1 second in set intervals to see how the data is captured given less of a window and lastly incorporating some noise into the reference data and comparing its reconstruction.

In this section we will only be showing the results of EDMD using a second order polynomial basis lift on a pendulum system. This setup was chosen since it had an accurate reconstruction model but also had some noise to enhance the visibility of incurred errors from that variances in the simulation.

### 3.5.1 Sampling Rate

In this section we altered the sampling rate for a second order polynomial basis lifted pendulum data with a full state reconstruction. In Fig. 3.15 and 3.16 we tested with an increased sampling rate of 1000 Hz over the same duration as Fig. 3.5. In Fig. 3.17 and 3.18 we tested with a decreased sampling rate of 10 Hz where we have little to no difference in the recon-

struction error of the system. In Fig. 3.21 and 3.22 while we see a significant change in the shape of the reference and reconstruction data we do not see any significant changes in the reconstruction of the stated data and the drifts caused by numerical errors is also correctly captured.

We can see in these variations that the reconstruction is quite accurate for both the controlled and uncontrolled data. We can also see that the tapering of the controlled data being cut off in Fig. 3.28 has almost not effect in the accuracy of the reconstruction of the state.

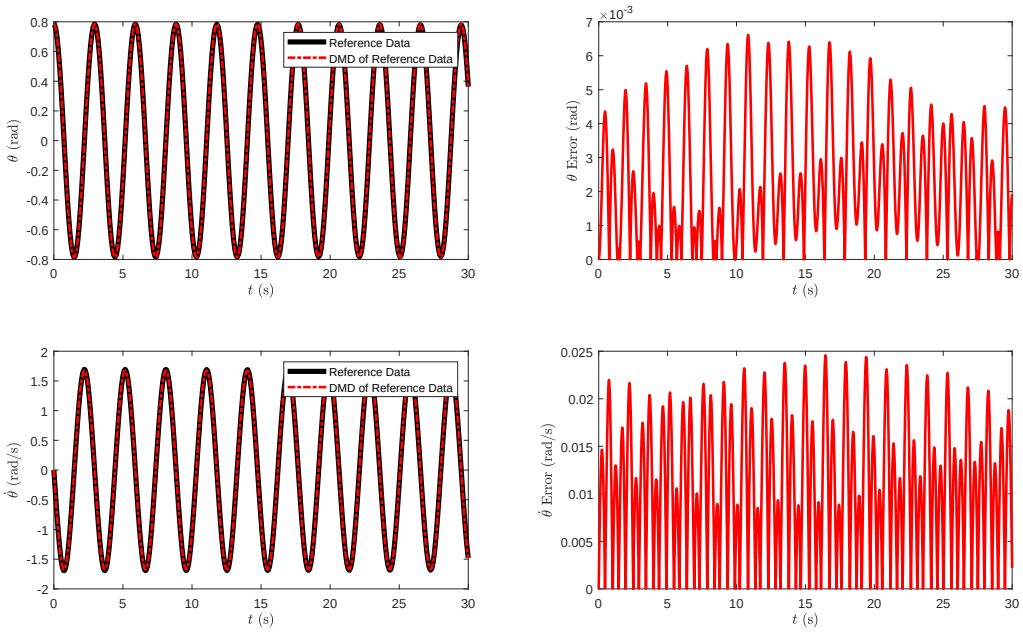


Figure 3.15: EDMD performed on a pendulum system with an uncontrolled data lifted by a second-order polynomial basis over a period of 30 seconds and at a 1000 Hz sampling rate.

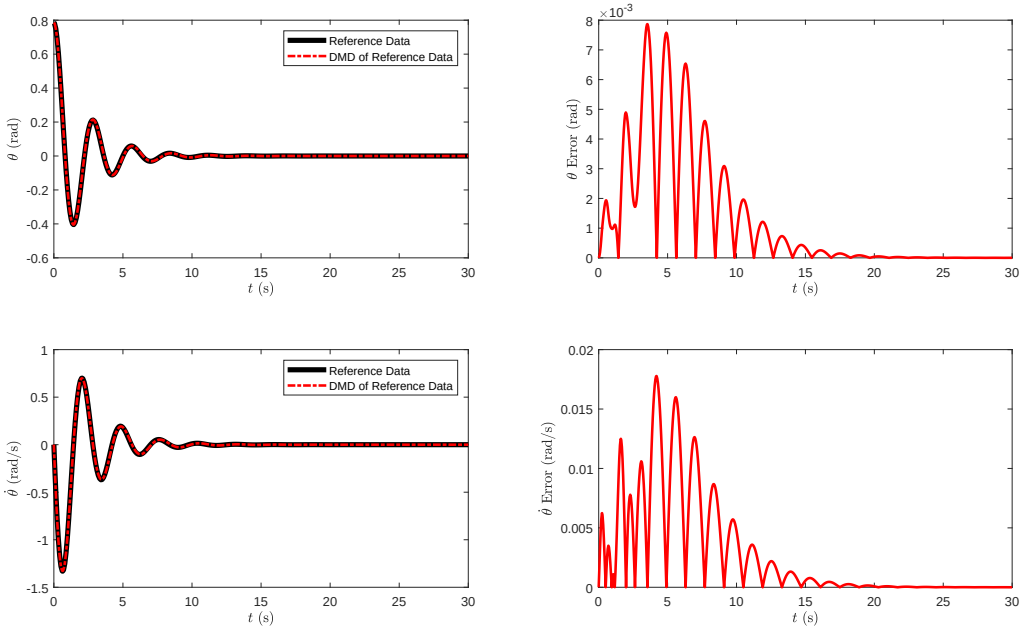


Figure 3.16: EDMD performed on a pendulum system with with a LQR controlled data set lifted by a second-order polynomial basis over a period of 30 seconds and at a 1000 Hz sampling rate.

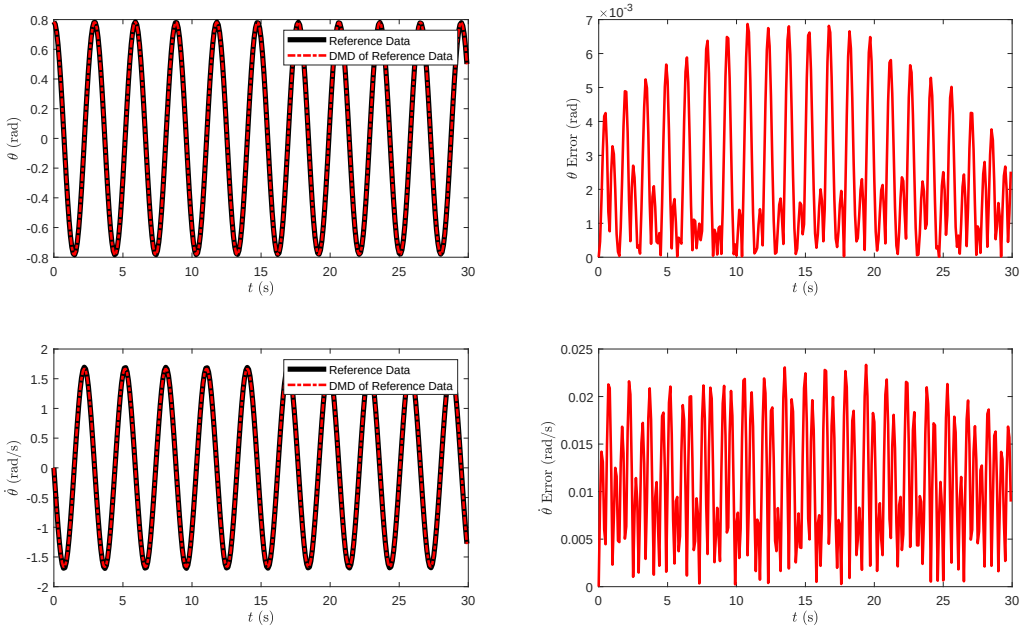


Figure 3.17: EDMD performed on a pendulum system with an uncontrolled data set lifted by a second-order polynomial basis over a period of 30 seconds and a 10 Hz sampling rate.

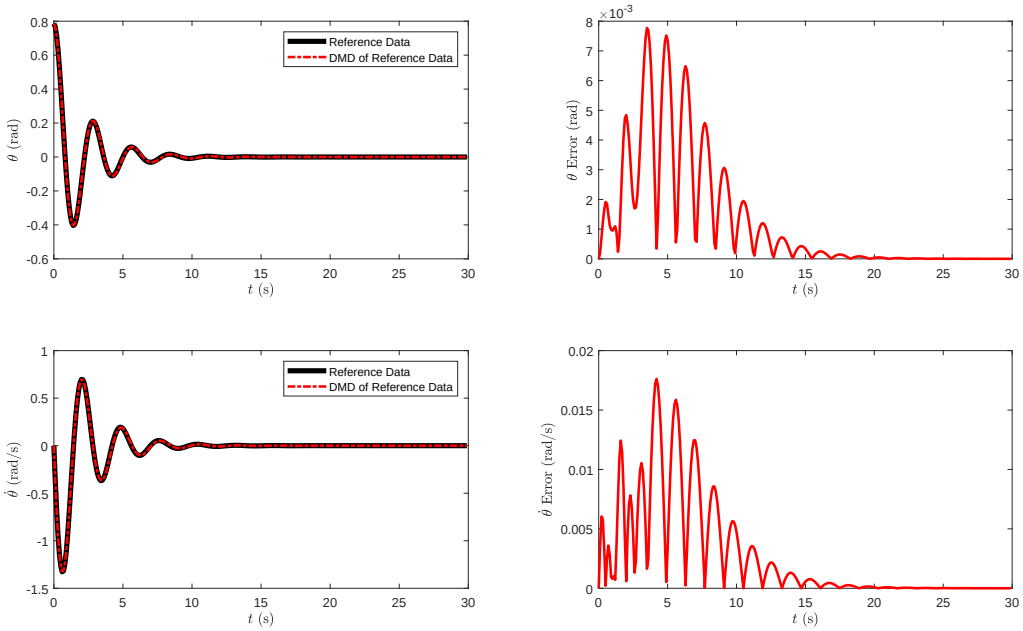


Figure 3.18: EDMD performed on a pendulum system with with a LQR controlled data set lifted by a second-order polynomial basis over a period of 30 seconds and a 10 Hz sampling rate.

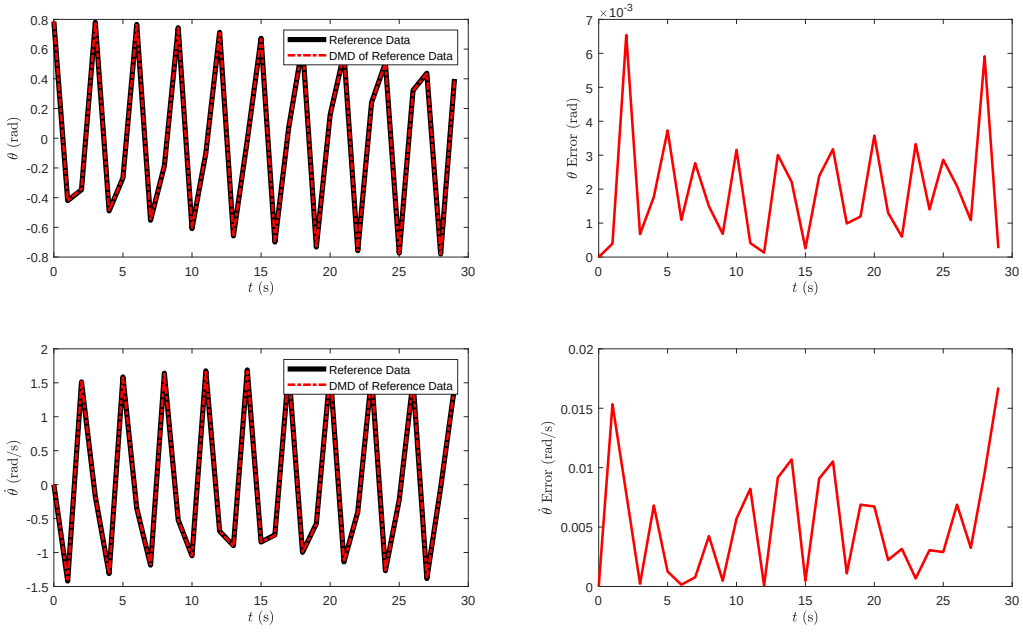


Figure 3.19: EDMD performed on a pendulum system with an uncontrolled data set lifted by a second-order polynomial basis over a period of 30 seconds and a 1 Hz sampling rate.

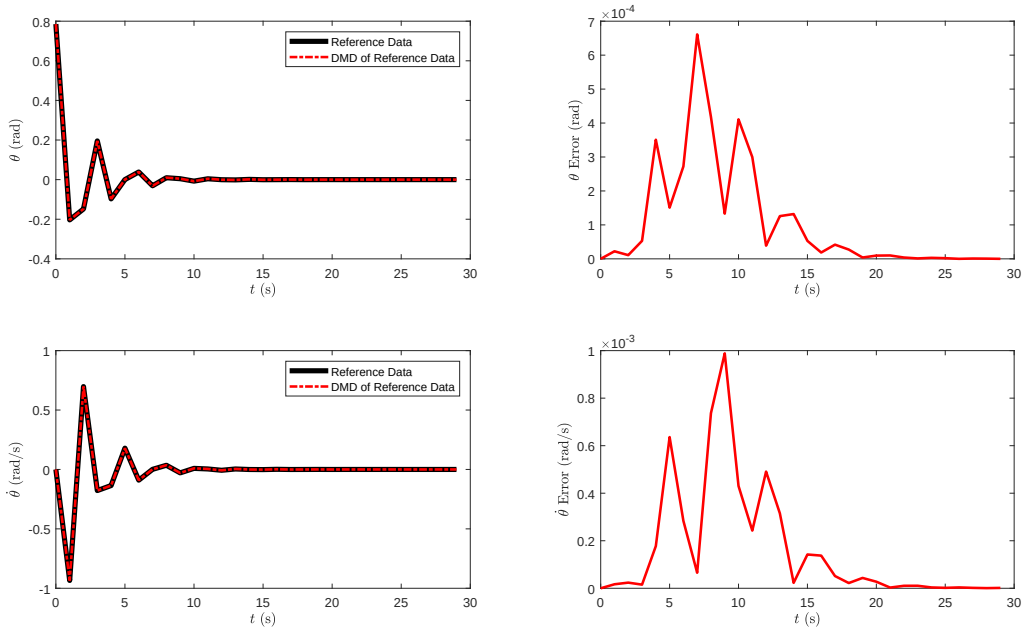


Figure 3.20: EDMD performed on a pendulum system with with a LQR controlled data set lifted by a second-order polynomial basis over a period of 30 seconds and a 1 Hz sampling rate.

### 3.5.2 Duration

In this section we decreased the window of the reference data to 1 second, 3 seconds, 10 and 15 second windows at 100 Hz on the pendulum system to show how the system behaviors are captured. We can see in these variations that the reconstruction is quite accurate for both the controlled and uncontrolled data. We can also see that the tapering of the controlled data being cut off in Fig. 3.28 has almost no effect in the accuracy of the reconstruction of the state.

Looking at the shape of the error we can see that the reconstruction of the smaller data samples that the error shapes have roughly the same behavior as when you compare Fig 3.22 to Fig 3.28 the leading maxima and minima are roughly the same showing that the reconstruction errors are mostly associated with the data itself rather than the duration of the sample set.

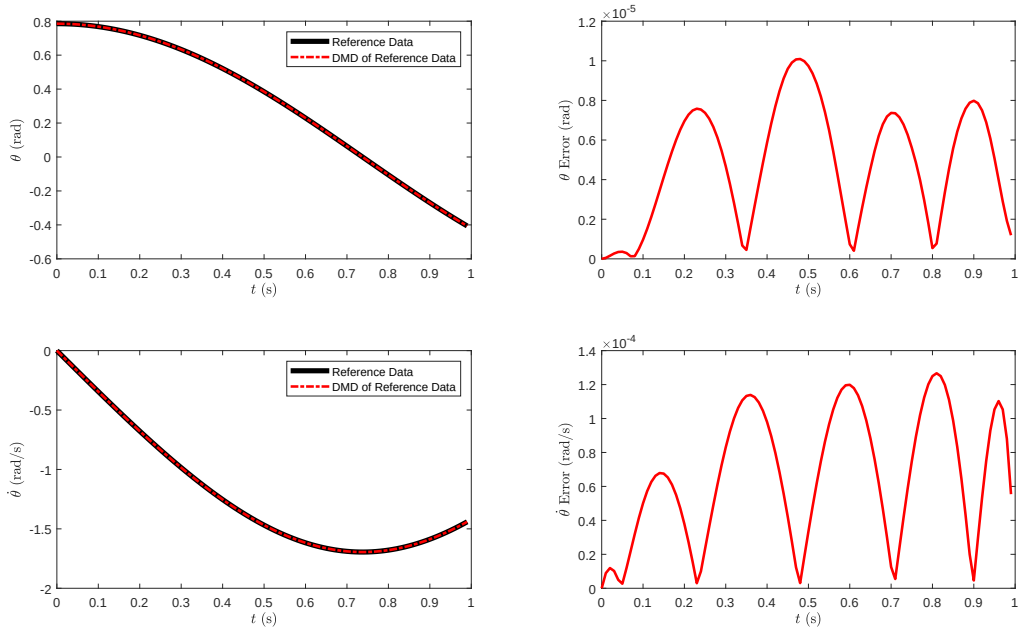


Figure 3.21: EDMD performed on a pendulum system with with an uncontrolled data set lifted by a second-order polynomial basis over a period of 1 second and a 100 Hz sampling rate.

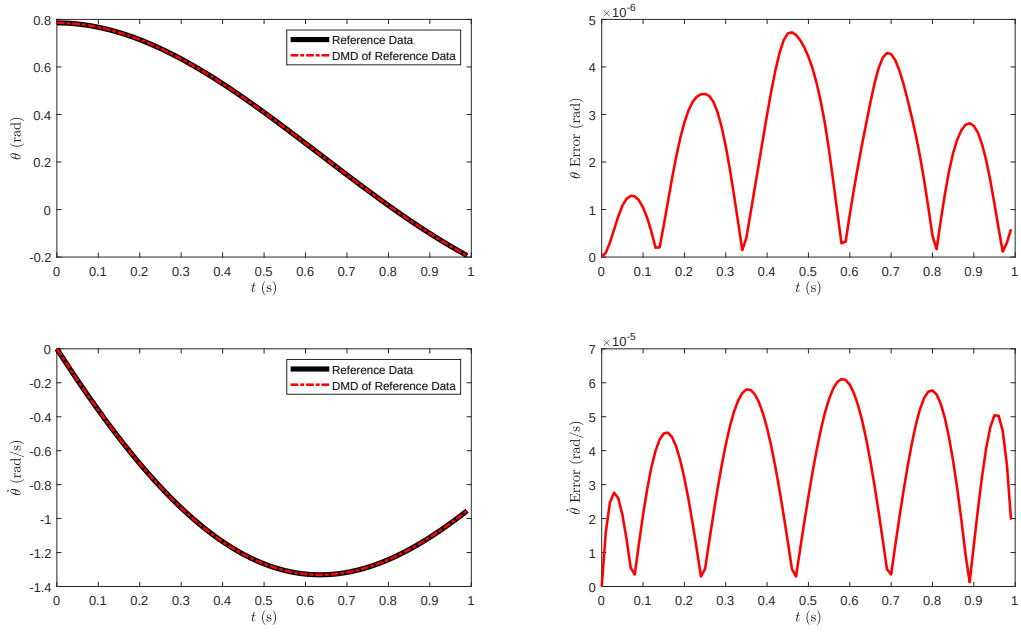


Figure 3.22: EDMD performed on a pendulum system with with a LQR controlled data set lifted by a second-order polynomial basis over a period of 1 second and a 100 Hz sampling rate.

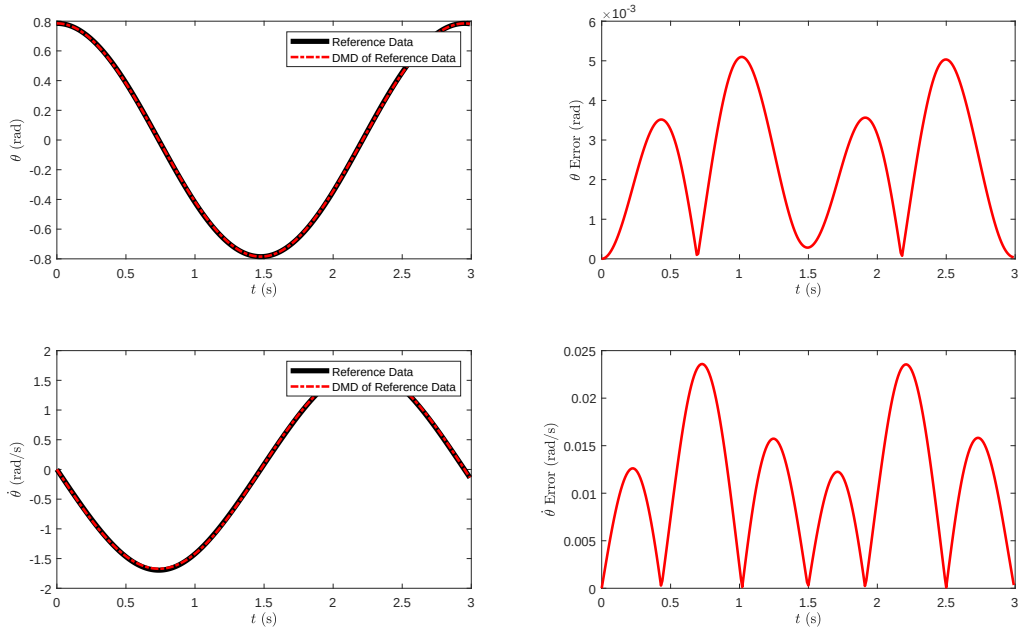


Figure 3.23: EDMD performed on a pendulum system with with an uncontrolled data set lifted by a second-order polynomial basis over a period of 3 seconds and a 100 Hz sampling rate.

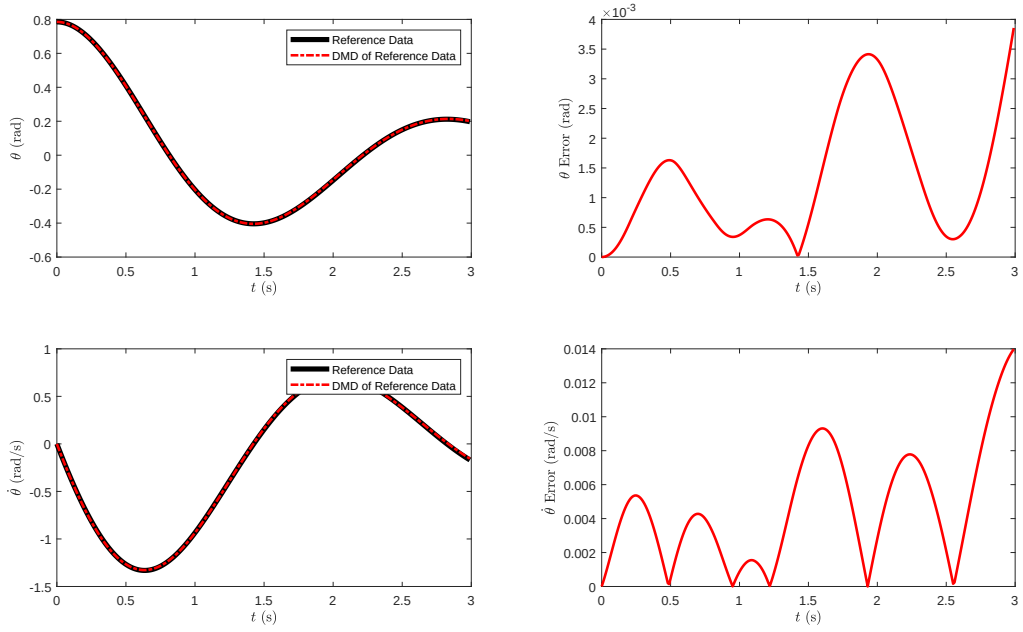


Figure 3.24: EDMD performed on a pendulum system with with a LQR controlled data set lifted by a second-order polynomial basis over a period of 3 seconds and a 100 Hz sampling rate.

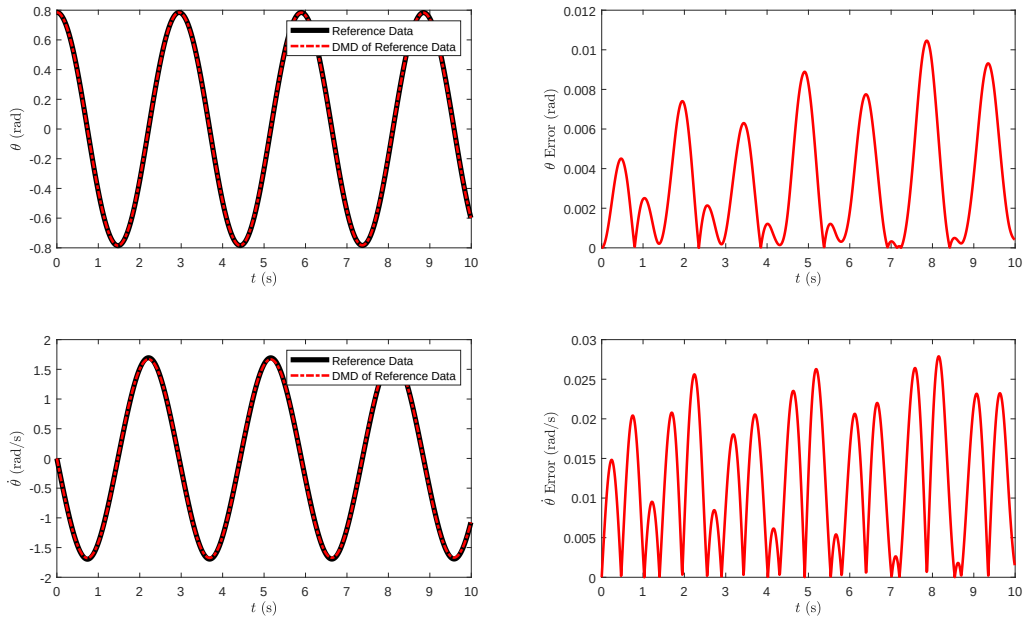


Figure 3.25: EDMD performed on a pendulum system with with an uncontrolled data set lifted by a second-order polynomial basis over a period of 10 seconds and a 100 Hz sampling rate.

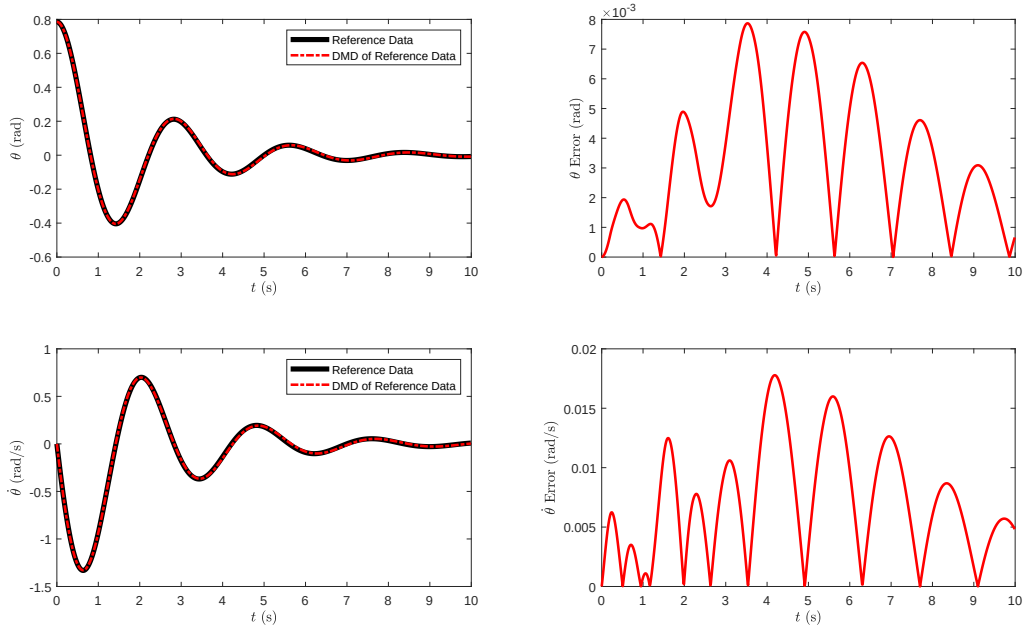


Figure 3.26: EDMD performed on a pendulum system with with a LQR controlled data set lifted by a second-order polynomial basis over a period of 10 seconds and a 100 Hz sampling rate.

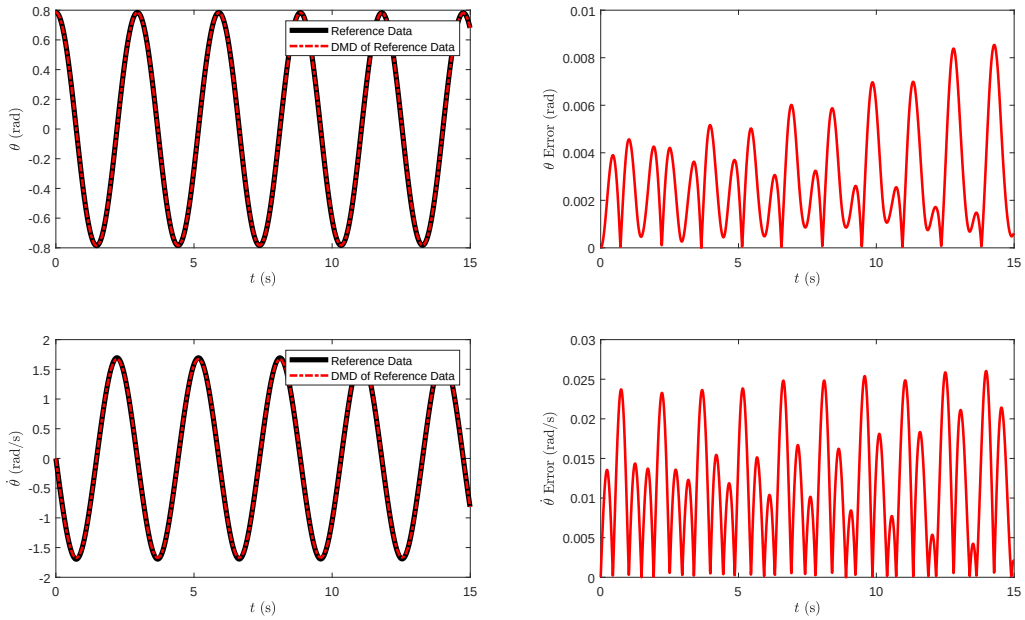


Figure 3.27: EDMD performed on a pendulum system with with an uncontrolled data set lifted by a second-order polynomial basis over a period of 15 seconds and a 100 Hz sampling rate.

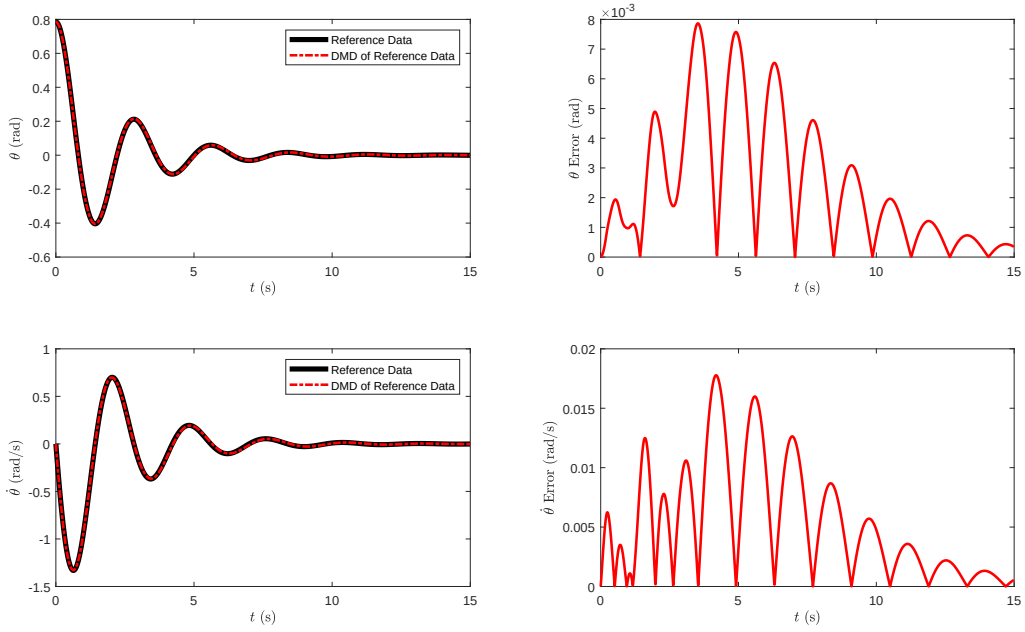


Figure 3.28: EDMD performed on a pendulum system with with a LQR controlled data set lifted by a second-order polynomial basis over a period of 15 seconds and a 100 Hz sampling rate.

### 3.5.3 Noisy

In this section we injected some nose into the reference data.

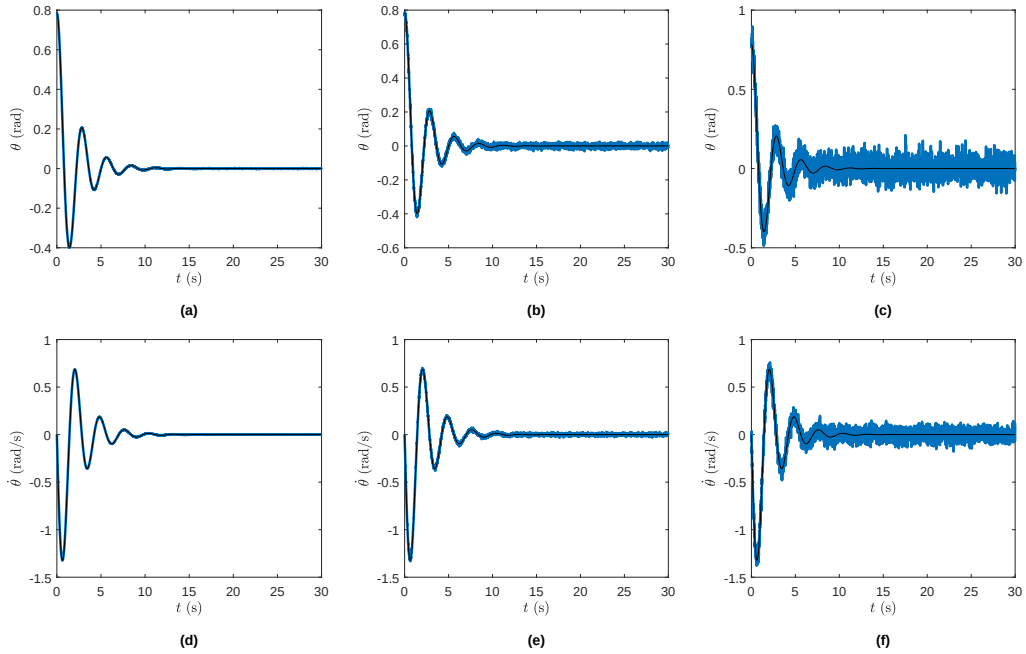


Figure 3.29: Noise sample of uncontrolled inverted pendulum over a period of 30 seconds at a 1 millisecond sampling rate. Plot (a) and (d) have a noise magnitude standard deviation of 0.001, plot (b) and (e) have a noise magnitude standard deviation of 0.01 and plot (c) and (f) have a noise magnitude standard deviation of 0.05

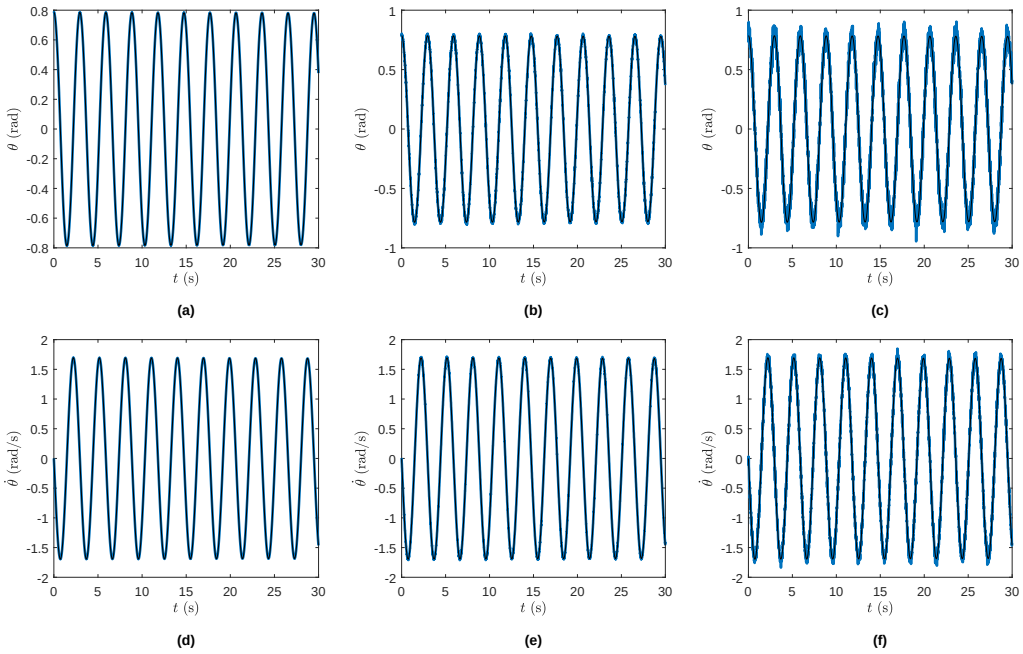


Figure 3.30: Noise sample of controlled inverted pendulum over a period of 30 seconds at a 1 millisecond sampling rate. Plot (a) and (d) have a noise magnitude standard deviation of 0.001, plot (b) and (e) have a noise magnitude standard deviation of 0.01 and plot (c) and (f) have a noise magnitude standard deviation of 0.05

We can see in Fig. 3.29 and 3.30 that in our analysis we used three different sets of noise on the pendulum system that alter the shape of the original data set. This noise was normally distributed before EDMD with standard deviations of 0.001, 0.01 and 0.05 to each state. Below a the lowest noise applied there was no noticeable difference in the reconstruction error and above a noise standard deviation of 0.05 the uncontrolled data reconstruction would level to the origin faster as would the controlled data providing similar if not worse reconstruction of the reference state data.

Looking at figures 3.31 through 3.36 we can see that there is a loss in capturing the dynamics immediately with the 0.001 noise injection where the dynamics appear to decay to the origin as we increase the magnitude of the noise on the system. This shows how the noise can drastically affect the eigenvectors of the system dynamics and the representation of the periodic behavior of the pendulum system. It is of interest to note that the despite each state receiving different noise inputs within and between tests that the shapes of the reconstructed systems follow the same pattern.

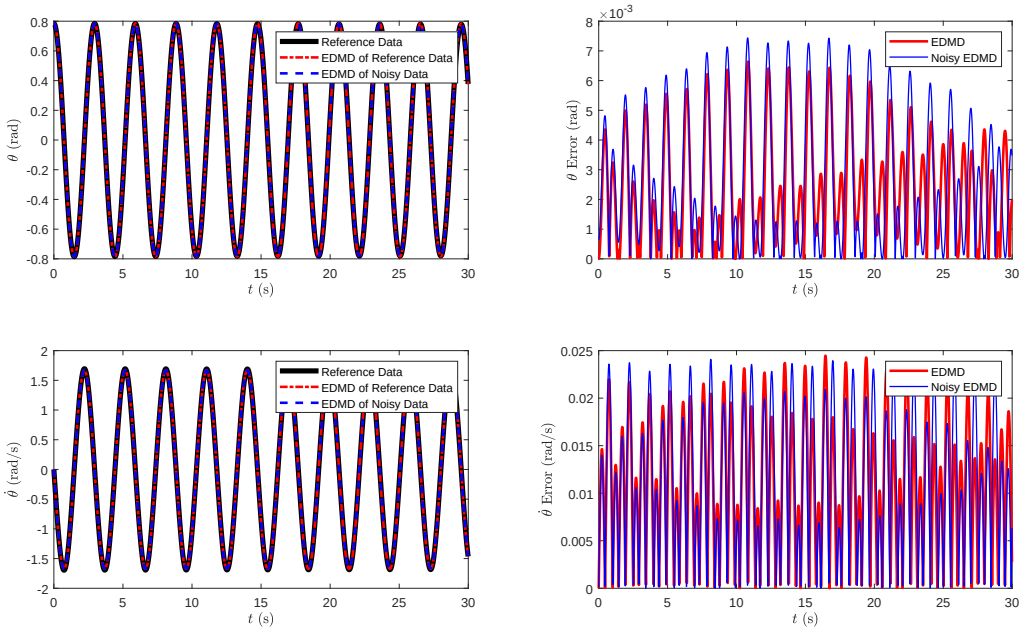


Figure 3.31: EDMD performed on a pendulum system with with uncontrolled data lifted by a second-order polynomial basis over a period of 30 seconds and a 100 Hz sampling rate with simulated noise with a standard deviation of 0.001 of each respective state.

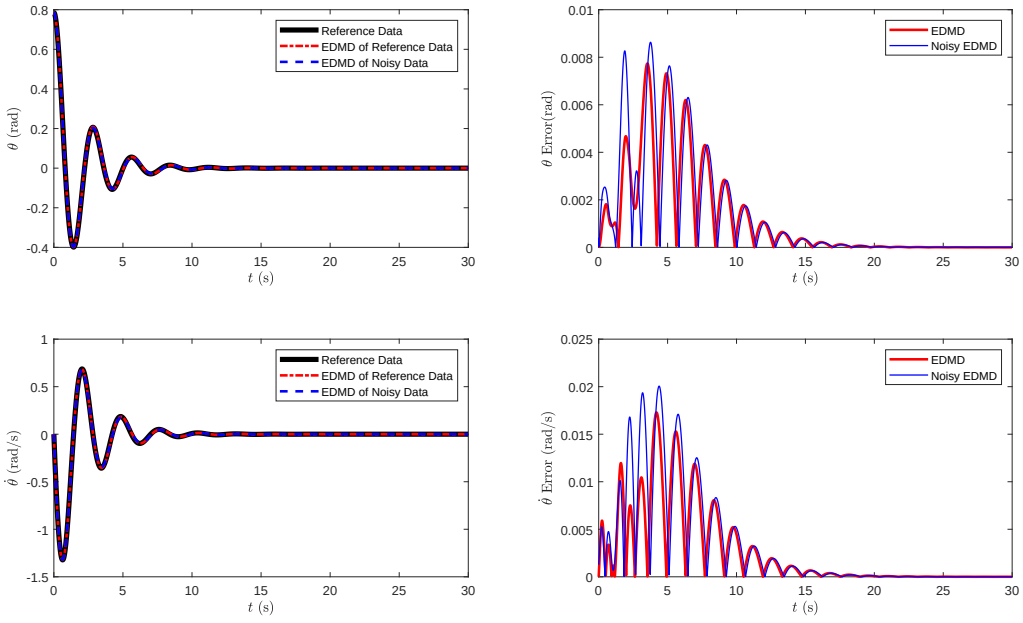


Figure 3.32: EDMD performed on a pendulum system with with a LQR controlled data set lifted by a second-order polynomial basis over a period of 30 seconds and a 100 Hz sampling rate with simulated noise with a standard deviation of 0.001 of each respective state.

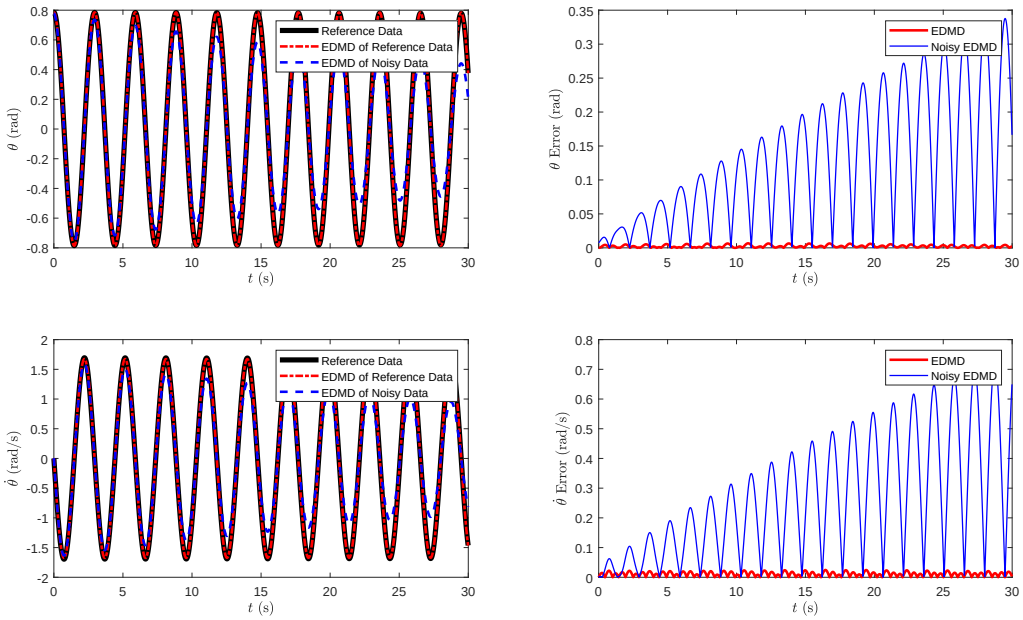


Figure 3.33: EDMD performed on a pendulum system with with uncontrolled data lifted by a second-order polynomial basis over a period of 30 seconds and a 100 Hz sampling rate with simulated noise with a standard deviation of 0.01 of each respective state .

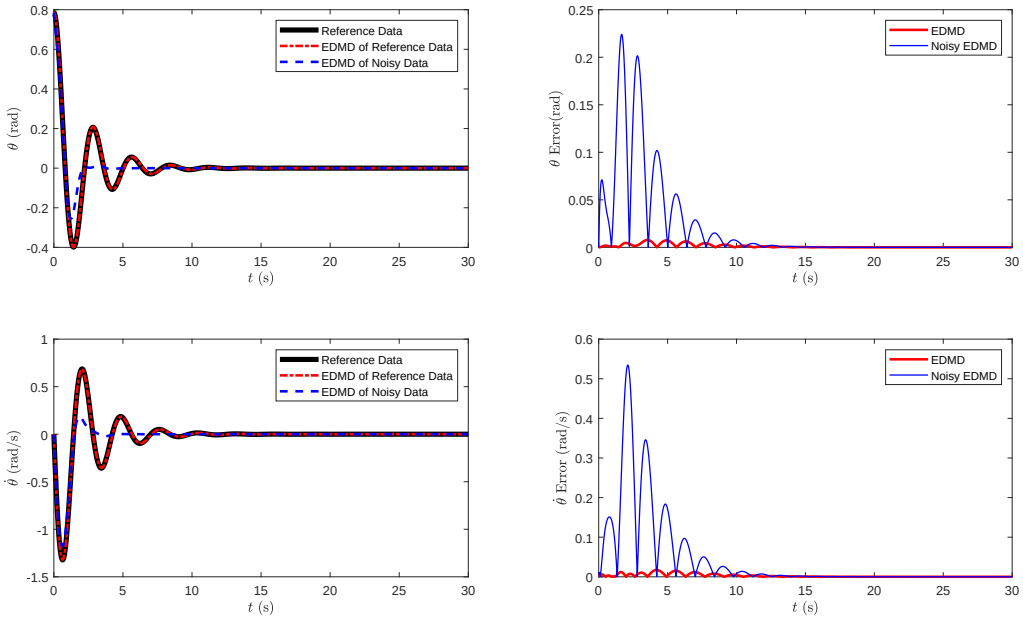


Figure 3.34: EDMD performed on a pendulum system with with a LQR controlled data set lifted by a second-order polynomial basis over a period of 30 seconds and a 100 Hz sampling rate with simulated noise with a standard deviation of 0.01 of each respective state.

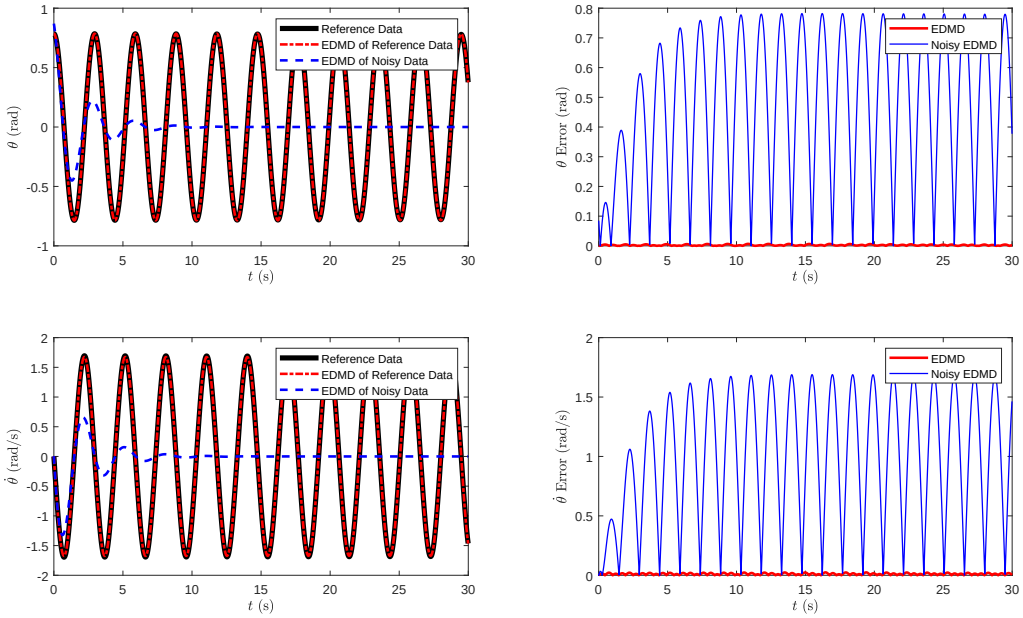


Figure 3.35: EDMD performed on a pendulum system with with uncontrolled data lifted by a second-order polynomial basis over a period of 30 seconds and a 100 Hz sampling rate with simulated noise with a standard deviation of 0.05 of each respective state .

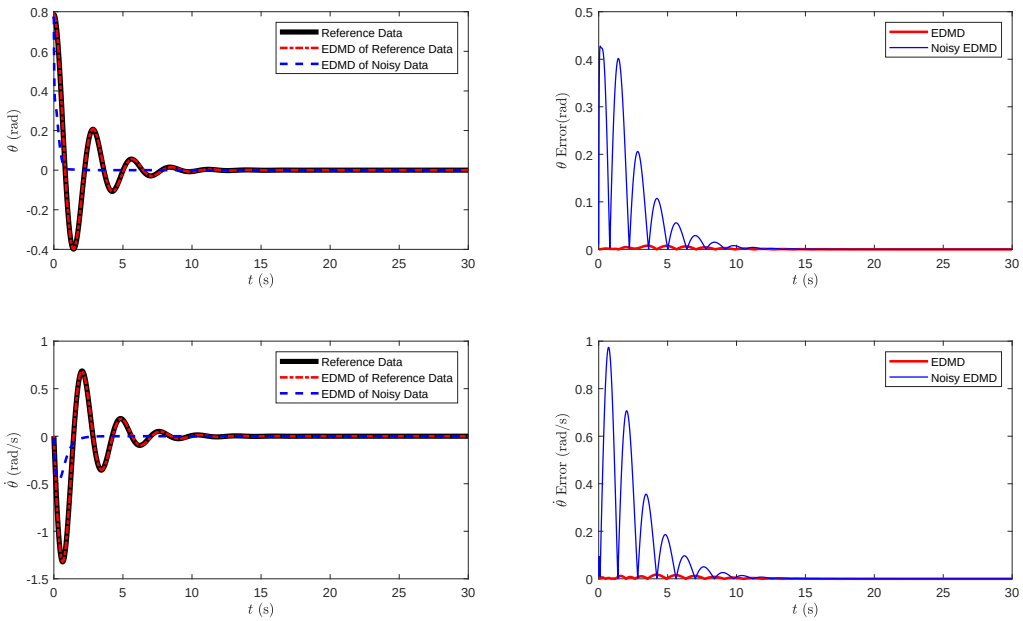


Figure 3.36: EDMD performed on a pendulum system with with a LQR controlled data set lifted by a second-order polynomial basis over a period of 30 seconds and a 100 Hz sampling rate with simulated noise with a standard deviation of 0.05 of each respective state.

# CHAPTER 4
# CONCLUSION

In this work we evaluated the ability to use Koopman operator theory to recreate models of a simple, pendulum and cart-pole system from varying qualities and quantities of data. Using the data driven method of dynamic mode decomposition and its higher dimensional variant, extended dynamic mode decomposition, we evaluated the fidelity of the models created from these algorithms for creating a linear dynamical system. Our findings looked into how the spread of data, quantity and the quality of the data affects the modeling process and how it affects two similar dynamical systems with differing degrees of freedom.

## 4.1 Evaluation of Koopman Reconstruction

### 4.1.1 Inverted Pendulum

We were able to find the Koopman operator for the inverted pendulum system using DMD and EDMD under several variations. We captured the data and produced several high fidelity models using the Koopman operator using both controlled and uncontrolled data from this system. This study showed a robustness in the strength of EDMD when exploring variances in the resolution, length and clarity of the data sets that were used to find the Koopman operators of this system. We found that for a sufficient duration the sampling rate in which the data is collected does not significantly alter the reconstruction of the system dynamics using the Koopman operator as long as the sampling rate is constant. Additionally, we found that the duration in which data was collected also did not significantly affect the fidelity of the Koopman reconstruction however these smaller sample sets will probably not be sufficient to model the systems at times significantly outside the range of the shorter sample sets.

When we applied noise to the reference data to learn the Koopman operator of the system we found that noise with a standard deviation greater than 0.001 of each individual state caused a decay to be captured in the uncontrolled data. In the controlled data we can see that as we increase the amount of noise on the system the reconstruction creates a dampening effect in the reconstruction. While our results show a similar decay to zero in the controlled state, if the goal we were using LQR to stabilize the system to was a larger or smaller value, the reconstruction would be attracted to that respective value.

The EDMD reconstructions agreed with previous works on this algorithm for finding the

Koopman operator. We can see improved fidelity in the model as we increase the original state space for the Koopman reconstruction with a stronger model when using a Fourier basis function to lift the reference data. When we begin truncating the lifted state to smaller ranks of SVD in the EDMD algorithm we noticed that there is sometimes important data lost in the reconstruction leading to weaker models in systems lifted using a Fourier basis function. More accurate, truncated EDMD reconstructions can be achieved by using the magnitude of the Koopman eigenvalues instead of the desired number of states should be considered.

### 4.1.2 Cart-Pole

In this work we put the cart-pole system through the same testing parameters as the simple pendulum. For the uncontrolled data sets both DMD and EDMD were unable to correctly capture the dynamics of the system. While this initially appears to be a result of the bounds of the data used in DMD, looking further into the matter showed that this was not a contributing factor to the algorithm's inability to correctly capture the system dynamics. As described in [9], sharp transient dynamics may not be successfully captured in the eigen decomposition of the data leading to a low fidelity reconstruction if at all. For the controlled data we can see more promising results however this initial spikes due to the control input causes some loss in the reconstruction which is not dependent on the initial magnitude of the change. When we evaluated the aforementioned parameters we tested for the simple pendulum system, the DMD and EDMD algorithms for finding the Koopman operator for this system showed similar variances with the changes.

## 4.2 Future Work

Future work on the usage of the Koopman operator on like systems introduced in this work includes evaluation of different methods of lifting the system dynamics. Further exploration is required of the effects of truncation when approximating the Koopman operator through EDMD as well as the method of which is chosen to truncate the states. Fourier series approximation through Direct Fourier Transforms and other polynomial approximations through Hermite polynomials and using the Jacobian are the next target of investigation. Additionally other data driven methods of evaluating the Koopman operator are being explored for the mentioned systems using methods such as Koopman reduced order nonlinear identification and control and Sparse identification of nonlinear dynamics (SINDy). In parallel, methods of using the approximated linear dynamics in other applications that rely on linear systems

will be looked into such as implementation with Kalman filters and other Bayesian filtering methods. Alternate perspectives are being considered on how to generate a control matrix from data, current prospects include the DMD variant for control among others. Once linear control matrices for the Koopman defined system can be found, As with the original motivation behind this work, once alternative methods of finding the Koopman operator have been explored we will use this theory to generated models and controls for quadcopter systems.

### 4.2.1 Submitted Work

In the process of producing this work three conference papers were submitted. The first paper discussed the process in which we generated data and used DMD and EDMD to find the Koopman operator as described in Chapter 3 and compared the accuracy of four different lifitng functions that were also described in the aformentioned section. [32]

In parallel to this work on the Koopman operator, two additional works has been produced and submitted regarding other aspects of guidence, navigation and control. In S. Shriwastav et al., [33] where trajectories were planned by visiting specific nodes to map a flow field using compressed sensing algorithms. Once these trajectories were found they were performed by nano-quadcopters in the RAN lab for experimental validation. In [34], Snyder et al., developed a set of algorithms for a unmanned aerial vehicle to explore a map while trying to explore as many high value areas as possible while maintaining enough power to return to the vehicle's starting point. All three of these works have been submitted to their respictive conferences and are awaiting review and publication.

# BIBLIOGRAPHY


[1] B. O. Koopman. Hamiltonian systems and transformation in hilbert space. *Proceedings of the National Academy of Sciences*, 17(5):315–318, 1931.

[2] B. O. Koopman and J. V. Neumann. Dynamical systems of continuous spectra. *Proceedings of the National Academy of Sciences of the United States of America*, 18(3):255–263, 1932.

[3] I. Mezic. Spectral properties of dynamical systems, model reduction and decompositions. *Nonlinear Dynamics*, 41:309–325, 2005.

[4] Igor Mezić and Andrzej Banaszuk. Comparison of systems with complex behavior. *Physica D: Nonlinear Phenomena*, 197(1):101–133, 2004.

[5] Clarence Rowley, Igor Mezic, Shervin Bagheri, Philipp Schlatter, and Dan Henningson. Spectral analysis of nonlinear flows. *Journal of Fluid Mechanics*, 641:115 – 127, 12 2009.

[6] Peter J. Schmid. Dynamic mode decomposition of numerical and experimental data. *Journal of Fluid Mechanics*, 656:5–28, 2010.

[7] Taraneh Sayadi, PeterJ. Schmid, Joseph W. Nichols, and Parviz Moin. Reduced-order representation of near-wall structures in the late transitional boundary layer. *Journal of Fluid Mechanics*, 748:278–301, 2014.

[8] Dirk M. Luchtenburg Steven L. Brunton J. Nathan Kutz Jonathan H. Tu, Clarence W. Rowley. On dynamic mode decomposition: Theory and applications. *Journal of Computational Dynamics*, 1(2):391–421, 2014.

[9] J. Nathan Kutz, Steven L. Brunton, Bingni W. Brunton, and Joshua L. Proctor. *Dynamic Mode Decomposition: Data-Driven Modeling of Complex Systems*. SIAM-Society for Industrial and Applied Mathematics, Philadelphia, PA, USA, 2016.

[10] Eurika Kaiser, J Nathan Kutz, and Steven L Brunton. Data-driven discovery of koopman eigenfunctions for control. *Machine Learning: Science and Technology*, 2(3):035023, Jun 2021.

[11] S.L. Brunton and J.N. Kutz. *Data-Driven Science and Engineering: Machine Learning, Dynamical Systems, and Control*. Cambridge University Press, 2019.

[12] Gene F. Franklin, J. David Powell, and Abbas Emami-Naeini. Feedback control of dynamic systems (6th edition). 2010.

[13] Joshua Proctor, Steven Brunton, and J. Kutz. Generalizing koopman theory to allow for inputs and control. *SIAM Journal on Applied Dynamical Systems*, 17, 02 2016.

[14] Joshua L. Proctor, Steven L. Brunton, and J. Nathan Kutz. Dynamic mode decomposition with control. *SIAM Journal on Applied Dynamical Systems*, 15(1):142–161, 2016.

[15] Steven L Brunton, Bingni W Brunton, Joshua L Proctor, and J Nathan Kutz. Koopman invariant subspaces and finite linear representations of nonlinear dynamical systems for control. *PloS one*, 11(2):e0150171, 2016.

[16] Matthew O. Williams, Ioannis G. Kevrekidis, and Clarence W. Rowley. A data–driven approximation of the Koopman operator: Extending dynamic mode decomposition. *Journal of Nonlinear Science*, 25(6):1307–1346, Jun 2015.

[17] Milan Korda and Igor Mezić. Linear predictors for nonlinear dynamical systems: Koopman operator meets model predictive control. *Automatica*, 93:149–160, Jul 2018.

[18] Qianxiao Li, Felix Dietrich, Erik M. Bollt, and Ioannis G. Kevrekidis. Extended dynamic mode decomposition with dictionary learning: A data-driven adaptive spectral decomposition of the Koopman operator. *Chaos: An Interdisciplinary Journal of Nonlinear Science*, 27(10):103111, Oct 2017.

[19] Ian Abraham, Gerardo de la Torre, and Todd Murphey. Model-based control using koopman operators. *Robotics: Science and Systems XIII*, Jul 2017.

[20] Efrain Gonzalez, Moad Abudia, Michael Jury, Rushikesh Kamalapurkar, and Joel A. Rosenfeld. Anti-Koopmanism, 2021.

[21] A. Surana. Koopman operator based observer synthesis for control-affine nonlinear systems. In *2016 IEEE 55th Conference on Decision and Control (CDC)*, pages 6492–6499, 2016.

[22] Amit Surana and Andrzej Banaszuk. Linear observer synthesis for nonlinear systems using koopman operator framework. *IFAC-PapersOnLine*, 49(18):716 – 723, 2016. 10th IFAC Symposium on Nonlinear Control Systems NOLCOS 2016.

[23] M. Netto and L. Mili. A robust data-driven koopman kalman filter for power systems dynamic state estimation. *IEEE Transactions on Power Systems*, 33(6):7228–7237, 2018.

[24] Enoch Yeung, Soumya Kundu, and Nathan Hodas. Learning deep neural network representations for koopman operators of nonlinear dynamical systems. In *2019 American Control Conference (ACC)*, pages 4832–4839, 2019.

[25] N. Fonzi, S. L. Brunton, and U. Fasel. Data-driven nonlinear aeroelastic models of morphing wings for control. *Proceedings of the Royal Society of London Series A*, 476(2239):20200079, July 2020.

[26] Alexandre Mauroy, Igor Mezic, and Yoshihiko Susuki. *The Koopman Operator in Systems and Control Concepts, Methodologies, and Applications: Concepts, Methodologies, and Applications*. 01 2020.

[27] Steven L. Brunton, Bingni W. Brunton, Joshua L. Proctor, and J. Nathan Kutz. Koopman invariant subspaces and finite linear representations of nonlinear dynamical systems for control. *PLOS ONE*, 11(2):e0150171, Feb 2016.

[28] Igor Mezic. Spectral properties of dynamical systems, model reduction and decompositions. *Nonlinear Dynamics*, 41:309–325, 08 2005.

[29] Igor Mezic. Analysis of fluid flows via spectral properties of the koopman operator. *Annual Review of Fluid Mechanics*, 45:357–378, 01 2013.

[30] Jonathan H. Tu, Clarence W. Rowley, Dirk M. Luchtenburg, Steven L. Brunton, and J. Nathan Kutz. On dynamic mode decomposition: Theory and applications. *Journal of Computational Dynamics*, 1(2):391–421, 2014.

[31] Matan Gavish and David L. Donoho. The optimal hard threshold for singular values is 4/sqrt(3). *IEEE Transactions on Information Theory*, 60(8):5040–5053, 2014.

[32] Gregory Snyder and Zhuoyuan Song. Koopman operator theory for nonlinear dynamic modelling using dynamic mode decomposition. In *American Control Conference (ACC)*, 2022. (Submitted).

[33] Sachin Shriwastav, Gregory Snyder, and Zhuoyuan Song. Dynamic compressed sensing of unsteady flows with a mobile robot. In *American Control Conference (ACC)*, 2022. (Submitted).

[34] Gregory Snyder, Sachin Shriwastav, Dylan Morrison-Fogel, and Zhuoyuan Song. Uav path planning for optimal coverage of areas with nonuniform importance. In *AIAA SciTech Forum*, 2022. (Awaiting Publication).

[35] Steven L. Brunton, Joshua L. Proctor, and J. Nathan Kutz. Discovering governing equations from data by sparse identification of nonlinear dynamical systems. *Proceedings of the National Academy of Sciences*, 113(15):3932–3937, Mar 2016.

[36] Sebastian Thrun, Wolfram Burgard, and Dieter Fox. *Probabilistic Robotics (Intelligent Robotics and Autonomous Agents)*. The MIT Press, 2005.

[37] Urban Fasel, Nicola Fonzi, and Steven L. Brunton. Data-driven nonlinear aeroelastic models of morphing wings for control. In *APS Division of Fluid Dynamics Meeting Abstracts*, APS Meeting Abstracts, page K09.002, January 2020.

[38] Enoch Yeung, Soumya Kundu, and Nathan Hodas. Learning deep neural network representations for koopman operators of nonlinear dynamical systems. 2017.

[39] Steven L. Brunton, Bingni W. Brunton, Joshua L. Proctor, Eurika Kaiser, and J. Nathan Kutz. Chaos as an intermittently forced linear system. *Nature Communications*, 8(1), May 2017.

[40] Ioannis G. Kevrekidis Matthew O. Williams, Clarence W. Rowley. A kernel-based method for data-driven koopman spectral analysis. *Journal of Computational Dynamics*, 2(2):247–265, 2015.

[41] Giorgos Mamakoukas, Maria Castano, Xiaobo Tan, and Todd Murphey. Derivative-based koopman operators for real-time control of robotic systems. *IEEE Transactions on Robotics*, 04 2021.